Limnol. Oceanogr., 56(1), 2011, 303–322

doi:10.4319/lo.2011.56.1.0303

Seasonal variability of the inorganic carbon system in the Amundsen Gulf region of the southeastern Beaufort Sea

E. H. Shadwick,[a,*] H. Thomas,[a] M. Chierici,[b] B. Else,[c] A. Fransson,[d] C. Michel,[e] L. A. Miller,[f] A. Mucci,[g] A. Niemi,[e] T. N. Papakyriakou,[c] and J.-É. Tremblay[h]

[a] Department of Oceanography, Dalhousie University, Halifax, Nova Scotia, Canada
[b] Department of Chemistry, University of Gothenburg, Göteborg, Sweden
[c] Center for Earth Observation Science, University of Manitoba, Winnipeg, Manitoba, Canada
[d] Department of Earth Sciences, University of Gothenburg, Göteborg, Sweden
[e] Freshwater Institute, Fisheries and Oceans Canada, Winnipeg, Manitoba, Canada
[f] Institute of Ocean Sciences, Fisheries and Oceans Canada, Sidney, British Columbia, Canada
[g] Department of Earth and Planetary Sciences, McGill University, Montreal, Québec, Canada
[h] Department de Biologie, Université Laval, Québec, Québec, Canada

Abstract

During a year-round occupation of Amundsen Gulf in the Canadian Arctic Archipelago dissolved inorganic and organic carbon (DIC, DOC), total alkalinity (TA), partial pressure of CO_2 (pCO_2) and related parameters were measured over a full annual cycle. A two-box model was used to identify and assess physical, biological, and chemical processes responsible for the seasonal variability of DIC, DOC, TA, and pCO_2. Surface waters were undersaturated with respect to atmospheric CO_2 throughout the year and constituted a net sink of 1.2 mol C m^{-2} yr^{-1}, with ice coverage and ice formation limiting the CO_2 uptake during winter. CO_2 uptake was largely driven by under ice and open-water biological activity, with high subsequent export of organic matter to the deeper water column. Annual net community production (NCP) was 2.1 mol C m^{-2} yr^{-1}. Approximately one-half of the overall NCP during the productive season (4.1 mol C m^{-2} from Apr through Aug) was generated by under-ice algae and amounted to 1.9 mol C m^{-2} over this period. The surface layer was autotrophic, while the overall heterotrophy of the system was fueled by either sedimentary or lateral inputs of organic matter.

The record low sea-ice coverage in the Arctic in 2007 contributes to a growing body of evidence supporting global climate change (Moritz et al. 2002; Maslanik et al. 2007; Stroeve et al. 2007). The Arctic Ocean is an ecologically sensitive area where the early detection of climatic changes may be possible (Serreze et al. 2000). Many arctic marine ecosystems are ice-dependent and are vulnerable to small shifts in ambient water temperature (Vallières et al. 2008). Furthermore, this region is also chemically sensitive due to the relatively high ratio between dissolved inorganic carbon and alkalinity, and the correspondingly weak buffer capacity of the waters (Orr et al. 2005; Thomas et al. 2007), making the Arctic Ocean particularly responsive to increases in atmospheric CO_2, and especially susceptible to the effects of ocean acidification.

Coastal and shelf seas play an important role in the global carbon cycle by linking atmospheric, terrestrial, and open-ocean systems (Borges et al. 2005; Bozec et al. 2006). The role of the global coastal ocean in the uptake of atmospheric CO_2 has been under debate for some time (Walsh 1991; Frankignoulle and Borges 2001; Borges 2005). A recent synthesis by Chen and Borges (2009) suggests that high-latitude and temperate continental shelves tend to act as sinks for atmospheric CO_2, while tropical and subtropical coastal regions tend to act as sources of CO_2. The continental shelves make up roughly 50% of the surface area of the Arctic Ocean (Walsh 1991). At present, the Arctic continental shelves as a whole are undersaturated with respect to atmospheric CO_2, and may, therefore, potentially act as CO_2 sinks (Bates and Mathis 2009).

Compared to other open-ocean and coastal-ocean systems, the Arctic Ocean remains relatively poorly studied. Most observational studies have been limited to the summer and autumn seasons, when reduced ice-cover allows access (Macdonald et al. 2002; Mathis et al. 2007; Mucci et al. 2010). Observational data of the inorganic carbon system in the Arctic, particularly outside of the summer and autumn seasons are, therefore, sparse. Long-term time-series observations (Bates et al. 1996; Bates 2007), and repeat surveys (Sabine et al. 2004), which have much improved our understanding of the marine carbon cycle in open-ocean environments, have not yet been carried out in the Arctic Ocean.

We present dissolved inorganic carbon (DIC), total alkalinity (TA), and CO_2 partial pressure (pCO_2) measurements covering a complete annual cycle in the Amundsen Gulf region of the southeastern Beaufort Sea. These data were collected during the Circumpolar Flaw Lead System Study field program as part of the Canadian International Polar Year initiatives. These measurements were complemented by dissolved organic carbon (DOC) and nutrient data. The annual cycles of the inorganic carbon system parameters (DIC, TA, pCO_2, pH, and aragonite saturation state [Ω_{Ar}]) are presented, and their seasonal variations

* Corresponding author: Elizabeth.Shadwick@dal.ca

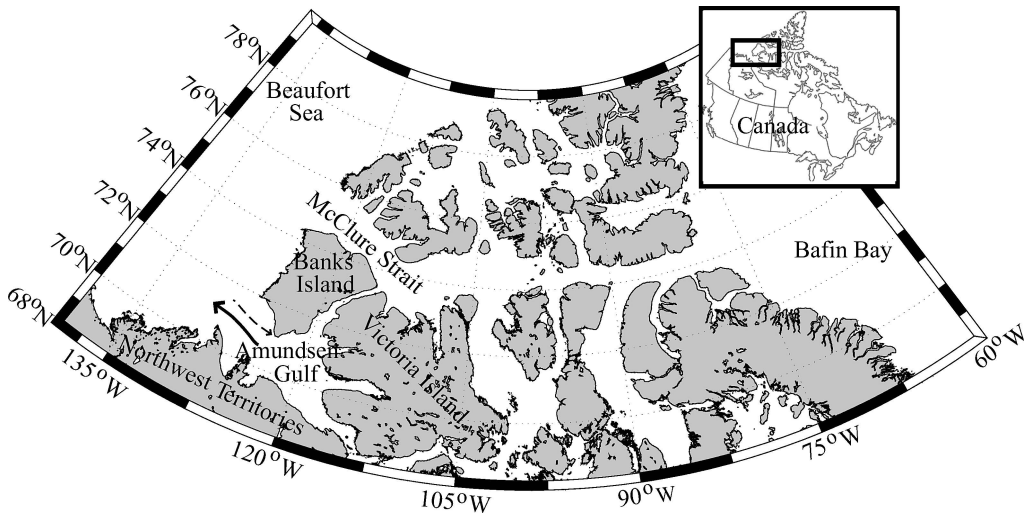

Fig. 1. Amundsen Gulf is located south of Banks Island in the southeastern Beaufort Sea. The arrows indicate schematically the flow of water in Amundsen Gulf; the dashed arrow represents the (weak) surface inflow from the west, while the solid arrow indicates the (stronger) subsurface flow toward the Beaufort Sea. The water transport follows Lanos (2009).

examined. The physical and biological processes responsible for the seasonal variations in water-column DIC are identified. A two-box model was constructed for the surface and subsurface layers in order to compute the monthly changes in DIC and TA due to: horizontal advection, vertical exchange between the boxes, air–sea exchange of CO_2, freshwater input from river runoff and sea-ice melt, and biological processes. Quantitative considerations of these processes yield an estimate of net community production for Amundsen Gulf on the basis of the inorganic carbon data collected in the region.

Oceanographic setting—Amundsen Gulf is bounded by Banks Island and the Beaufort Sea to the north, the Mackenzie Shelf to the west, the northern Canadian coast to the south, and the Arctic Archipelago to the east (Fig. 1). The anticyclonic Beaufort Gyre dominates the surface circulation in the Beaufort Sea, while the flow of subsurface waters is reversed and dominated by the cyclonic Beaufort Undercurrent (Aagaard 1984). This undercurrent forces waters of both Pacific and Atlantic origin to the east along the continental margin, providing (offshore) nutrients to the Arctic shelves (Macdonald et al. 1987; McLaughlin et al. 2004).

The Mackenzie Shelf, defined by the 200-m isobath, covers an area of 6.4×10^4 km^2 and is the largest shelf in the North American sector of the Arctic Ocean (Macdonald et al. 1987). The physical system dynamics on the shelf and surrounding waters can be described according to season. In winter, when the sea is ice-covered, the effect of wind-forcing is diminished, and density-driven flows, due to the release of brine during ice formation, can occur (Melling 1993). Ice breakup begins in the headwaters of the Mackenzie River in late April, moving progressively offshore and occurring on the shelf in mid-May (Carmack and MacDonald 2002). Between mid-May and June, there is a peak in river discharge; the Mackenzie River discharges roughly 2.9×10^{11} m^3 yr^{-1} (Stewart et al. 1998). As the breakup progresses, the land-fast ice disappears. During the summer months, the upper 20–30 m of the water column on the shelf and in the neighboring Amundsen Gulf are strongly stratified due to the combined effects of ice melt and inflow from the rivers (Carmack and MacDonald 2002). Throughout the summer and early autumn, storms mix the ice melt and runoff into the upper water column and weaken the stratification (Carmack and MacDonald 2002). Freeze-up begins in early to mid-October and is influenced by the summer ice conditions as well as the strength and direction of autumn winds (Stewart et al. 1998).

A recurrent feature of the central Arctic Ocean is the flaw-lead system. Polynyas are formed when the first-year pack is pushed away from the coast, leaving an area of open water behind. New ice is then free to form in this open-water area, and it will subsequently be pushed downwind toward the first-year pack ice. This creates the opening of a flaw lead in the winter season. The flaw lead is circumpolar, with interconnected polynyas forming in both the North American and Eurasian sectors of the Arctic (Barber and Massom 2006). The flaw-lead system is a site of high ice production and, consequently, there is potential for significant fluxes of brine from the continental shelf regions to the deeper basins (Barber and Massom 2006). In the Beaufort Sea, flaw leads form both along the northern Canadian and Alaskan coasts. Amundsen Gulf encompasses part of the Cape Bathurst polynya, which plays an important role in both the physical and biological processes in the system. In winter, this area of open water is a site of enhanced air–sea exchange and wind-forcing.

Water masses in the Arctic Ocean can be classified on the basis of their salinities (Aagaard et al. 1981; Aagaard and Carmack 1994; Mathis et al. 2005) and be simplistically represented by a three-layer system. The uppermost water column is dominated by the polar mixed layer (PML), a seasonally ice-covered, relatively low-salinity water mass ($S < 29$ [Hansell et al. 2004; Yamamoto-Kawai and Tanaka

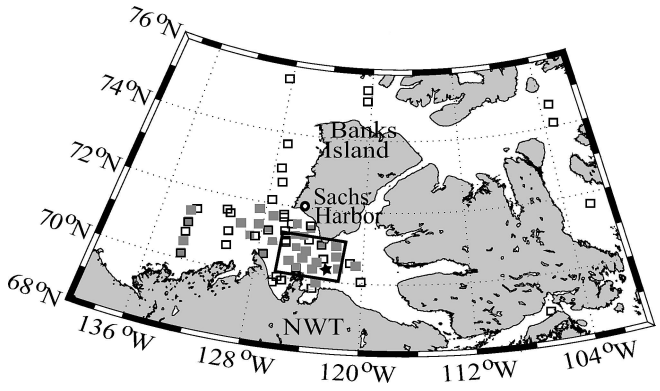

Fig. 2. Locations of sampling stations occupied from October 2007 to August 2008, and the limits of the budgeting area containing the surface and subsurface layers in Amundsen Gulf (box). The open black squares indicate stations occupied only once, and the closed gray squares indicate stations occupied more than once. The station indicated by the star (70.6°N, 122.4°W) was occupied many times and seasonal profiles from this location are presented in Fig. 7.

2005]). Immediately beneath the PML are the upper halocline waters (UHL) of Pacific origin (S = 33.1 [Macdonald et al. 2002; McLaughlin et al. 2004]), and the lower halocline waters (LHL) of Atlantic origin (S > 34).

Methods

Sampling and analytical measurements—Samples were collected on board the Canadian Coast Guard Ship *Amundsen* at roughly 50 stations in the Amundsen Gulf and Cape Bathurst polynya region of the Southeastern Beaufort Sea from October 2007 to August 2008. Approximately 2000 samples were collected from the entire water column, with higher vertical resolution within the euphotic zone, at all stations shown in Fig. 2. DIC and TA samples were tapped from 20-liter Niskin bottles mounted on a General Oceanics 24-bottle rosette fitted with a SeaBird conductivity temperature and depth sensor such that all chemical data were associated with high precision in situ temperature and salinity data. Following water collection, DIC and TA samples were poisoned with a saturated $HgCl_2$ solution to halt biological activity and stored in the dark, at 4°C, to await analysis.

All DIC and TA samples were analyzed on board by coulometric and potentiometric titration, respectively, using a Versatile Instrument for the Determination of Titration Alkalinity (VINDTA 3C; Marianda). Analytical methods for determination of DIC and TA have been fully described elsewhere (Johnson et al. 1993; Dickson et al. 2007). Routine analysis of Certified Reference Materials (provided by A. G. Dickson, Scripps Institution of Oceanography) ensured the accuracy of the DIC and TA measurements, whereas reproducibility was better than 1 μmol kg^{-1} and 2 μmol kg^{-1}, respectively. Following the determination of DIC and TA, the in situ partial pressure of CO_2 (pCO_2), pH (on the total scale), and aragonite saturation state (Ω_{Ar}) were computed, using the standard set of carbonate system equations, excluding nutrients, with the CO_2SYS program of Lewis and Wallace (1998). We used the equilibrium constants of Mehrbach et al. (1973) refit by Dickson and Millero (1987). The calcium (Ca^{2+}) concentration was assumed to be conservative and calculated from salinity.

In addition to rosette samples, sea-ice samples were collected for DIC and TA analysis from December to June. The ice was cored using a 9-cm-diameter corer (Mark II; Kovacks Enterprises), and the cores were immediately laid out on an area of ice that had been cleared of snow. The top, middle, and bottom 10 cm of the ice core were cut with a steel saw and placed in plastic bags (Tedlar ©) with a few microliters of saturated $HgCl_2$ solution to halt biological activity. The bag was sealed and air was withdrawn with a vacuum pump. These bags are gas-impermeable, with a clamp-type closure seal and small spigot for withdrawing air or water. The core sections were allowed to thaw, and the sample was then delivered directly from the bag, via the spigot, to the VINDTA for DIC and TA analysis as described above.

DOC samples were collected directly from the rosette. An acid-washed plastic syringe was mounted directly on the rosette port to collect the sample. The sample was then passed through an acid-washed Swinnex filter holder containing a 25-mm GF/F filter combusted at 450°C for 24 h. The first 5–10 mL of sample were discarded and the rest was poured into an acid-washed, precombusted borosilicate glass sample bottle. Each sample was immediately acidified with 200 μL of 50% H_3PO_4 40 mL^{-1} of sample. Samples were stored in amber glass vials sealed with an acid-washed teflon-lined septa and cap at 4°C. Measurements of DOC were carried out at the Freshwater Institute (Winnipeg, Manitoba, Canada) by high-temperature catalytic combustion, on a Shimadzu total organic carbon analyzer, according to procedures described by Dickson et al. (2007). DOC measurements were systematically checked against reference material low-carbon water (~ 2 μmol L^{-1} DOC) and deep Sargasso Sea reference water (~ 44–47 μmol L^{-1} DOC; provided by D. A. Hansell, University of Miami).

Nutrient samples were collected in acid-washed 15-mL polypropylene tubes. A 5.0-μm polycarbonate filter, mounted on a 47-mm filter holder, was attached directly to the sampling bottle to remove large particles. Colorimetric determinations of nitrate (NO_3^-), and silicate (Si) were performed on an Autoanalyzer-3 using routine methods (Grasshoff 1999). Analytical detection limits were 0.03 μmol L^{-1} for NO_3^-, and 0.1 μmol L^{-1} for Si.

The pCO_2 of the surface waters, for the computation of air–sea CO_2 fluxes, was measured using a continuous-flow equilibration system (Körtzinger et al. 1996). The detection of pCO_2 was made by a nondispersive infrared spectrometer (LiCor; LI-7000). The system was located in the engine room of the ship and the intake depth was ~ 3 m below the water surface. Measurements were made every minute and used to compute hourly averages. The system was calibrated daily with both a CO_2-free reference gas (N_2) and a CO_2 calibration gas provided by the U.S. National Oceanic and Atmospheric Administration. The temperatures at the intake and at the equilibrator were monitored

and the pCO_2 corrected to account for warming of the water in transit to the equilibrator. The data were corrected to in situ water temperature and to 100% humidity. The relationship between the underway pCO_2 measurements and the computed pCO_2 from discrete DIC and TA had a slope of roughly 1 : 1, which was significant at a confidence interval of > 99%. There was a slight positive offset (24×10^{-1} Pa), with the measured pCO_2 consistently higher than the computed values. Please note that the pCO_2 units used throughout the text (10^{-1} Pa) are equivalent to 1 microatmosphere or μatm. The offset was not statistically significant at a confidence interval of 90%. The most frequent problem encountered with the pCO_2 measurement was low flow through the system, typically caused by ice blockage in the intake line. A second (less common) problem was pressure spiking in the LI-7000 caused by blockages of the air lines. In both cases, these pCO_2 data were removed from the data set. Atmospheric pCO_2 was measured by a nondispersive open-path infrared CO_2 analyzer (LiCor; LI-7500) mounted on a meteorological tower on the ship's foredeck; air temperature was measured simultaneously. The atmospheric pCO_2 were processed to remove any measurements when the ship's exhaust might have been blowing over the tower. Hourly wind data measured by Environment Canada at the Sachs Harbor meteorological station (71.99°N, 125.25°W; *see* Fig. 2) at a height of 10 m were used to compute the gas transfer velocity using the formulation of Wanninkhof (1992).

Observed monthly changes—A region in central Amundsen Gulf was defined (from 122°W to 126°W, and from 70°N to 71.5°N), and divided into a surface and subsurface box (Figs. 1, 3). The surface box extends from 0 m to 50 m, whereas the subsurface box extends from 50 m to 300 m. The region covers an area of roughly 1.7×10^{10} m^2, and the surface and subsurface layers have a volume of $\sim 8.4 \times 10^{11}$ m^3 and 5.0×10^{12} m^3, respectively.

The annual cycles of DIC, TA, and other hydrographic variables, were reconstructed using data collected from October 2007 through August 2008. The temporal resolution chosen for the inorganic carbon budget presented here is monthly, and the September values were computed as the mean of the months of August and October. The DIC and TA concentrations were calculated for each station for both the upper (50 m) and lower (50–300 m) layers of the water column, and the average of all stations occupied in a given month was computed. Sampling took place weekly during the winter season, increased to twice weekly at the end of winter, then daily in the spring, summer, and autumn. Accordingly, the monthly DIC and TA concentrations computed for the surface and subsurface layers relied on 15–80 measurements, depending on the number of stations sampled per month and the vertical sampling resolution. We assume that the (computed) monthly mean observed DIC and TA concentrations are spatially homogeneous within the box and valid over the entire month. The changes in DIC and TA from one month to the next were computed by central difference and are denoted ΔDIC_{obs} and ΔTA_{obs}.

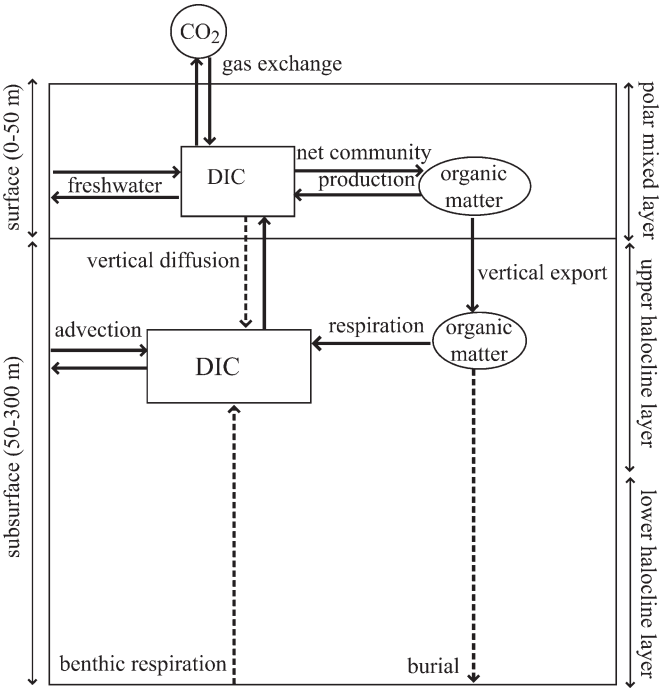

Fig. 3. Schematic representation of the two-box model used to compute the monthly changes in DIC (and TA) due to: lateral advection, freshwater input, air–sea exchange, vertical diffusion, and biology. The solid arrows indicate the dominant processes, while the dashed arrows represent secondary processes. The surface and subsurface layers are indicated (left-hand side) along with the locations of the dominant water masses (right-hand side).

Controls on DIC and TA—Changes in DIC and TA result from both physical and biological processes, with the latter having a lesser influence on TA than on DIC. Photosynthesis, respiration, and the formation of calcium carbonate ($CaCO_3$) are biologically mediated processes affecting both DIC and TA. Lateral and vertical advection, diffusion, and air–sea exchange of CO_2 are physical processes, the latter only influencing DIC concentration. A schematic representation of the two-box model used here and the processes affecting DIC concentration are shown in Fig. 3. The methods used to quantify the changes in DIC and TA due to the various processes are detailed in the following sections.

Advection—Contrary to the general west-to-east flow through the Arctic Archipelago (McLaughlin et al. 2005), recent in situ current measurements reveal that Amundsen Gulf exports more water to the Beaufort Sea than it receives (Lanos 2009). There is a weak surface flow (0.002 Sverdrup) into Amundsen Gulf from the west, but the circulation in the Gulf is dominated by a subsurface (below 50 m) flow with an annual mean value of 0.19 Sv toward the Beaufort Sea (Lanos 2009). Lanos (2009) suggests that the source of this water is McClure Strait and that it enters Amundsen Gulf from the north via the Prince of Wales Strait separating Banks and Victoria Island. The annual mean (net) water mass transports of Lanos (2009) were used to compute the contribution from lateral advection. The subsurface box receives 6.0×10^{12} m^3 of water per year

(5.0×10^{11} m^3 month^{-1}) flowing toward the Beaufort Sea. The surface box receives 6.3×10^{10} m^3 yr^{-1} (5.3×10^9 m^3 month^{-1}) from the Southern Beaufort Sea and the Mackenzie Shelf. The flushing time for the surface and subsurface boxes are roughly 14 months and 19 months, respectively. These values are in general agreement with literature values for the region (Bates and Mathis 2009). Multiplying the monthly volume transport by the DIC concentrations at stations located east of the subsurface box and west of the surface box gives the monthly contribution to the total change in DIC due to lateral advection. For the subsurface box, DIC concentrations for stations located just outside the area of interest were available for the months of February, April, and July 2008, and October 2007. It was assumed that the resulting differential between two locations, on the order of 35 μmol kg^{-1}, were valid over the season, (i.e., the same DIC concentration gradient was used for 3 months), and a fraction of the volume in the subsurface box was exchanged to reflect the 19-month flushing time. The advective change in TA was computed using the same method. A comparison of the surface DIC concentration inside the budgeting area with the surface concentration at stations immediately to the west revealed only a small concentration differential ($\sim$ 1 μmol kg^{-1}) throughout the year; the change in DIC and TA due to lateral advection in the surface layer was, therefore, neglected. Furthermore, the dominant effect in the surface box resulted from the addition or removal of freshwater, which was quantified independently.

Horizontal advection is not perfectly constrained in the model by empirically estimating horizontal transport with observed volume transport and horizontal concentration gradients. This method does not allow for a complete description of lateral processes in the region; however, the inclusion of the horizontal advection term in the one-dimensional approach used here allows changes due to transport and biology, often grouped together (Olsen et al. 2008; Omar et al. 2010), to be separated.

Freshwater—The surface waters of the Amundsen Gulf region, and the Arctic shelves in general, are heavily influenced by the addition (and removal) of freshwater, both from river runoff and from the melting (and formation) of sea-ice. Whereas runoff from the Mackenzie River contributes significantly to the input of terrestrial freshwater in the North American sector of the Arctic, much of this runoff is directed to the west, making its way into the surface waters of the Beaufort Gyre (Macdonald et al. 2002; Yamamoto-Kawai and Tanaka 2005). In contrast, the freshwater input to Amundsen Gulf is dominated by the formation and melting of sea-ice, with runoff playing a more minor role (Tremblay et al. 2008; Lanos 2009). This is also reflected in the lack of terrigenous material accumulation in the Amundsen Gulf sediments (Magen et al. 2010).

Salinity-dependent changes in DIC can be quantified by analyzing the relationship between the seasonal (or monthly) changes in DIC and salinity (Thomas and Schneider 1999; Bozec et al. 2006). Nevertheless, because changes in surface DIC concentration are also influenced by salinity-independent processes (i.e., air–sea exchange of CO_2, and biological activity), we quantified the influence of freshwater sources from the relationship between monthly changes in surface salinity and surface TA concentration. TA is also influenced by biological processes (nutrient consumption and regeneration through photosynthesis and respiration), but the effect is less significant than for DIC.

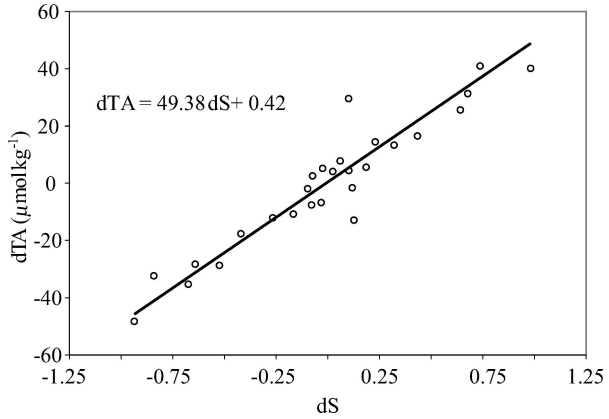

Fig. 4. Changes in surface TA (dTA) vs. changes in surface salinity (dS), for repeated, monthly, or seasonal, occupations of the same stations. The slope of the best-fit line ($n = 27$, $r^2 = 0.86$, $p < 0.01$) represents the change in TA due to the change in salinity. The changes in TA not due to changes in salinity (i.e., biological processes) are represented by the y-intercept, which in this case is not different from zero.

We computed the differences in surface salinity (dS) and surface TA (dTA), for all reoccupations of stations in the region. Changes are positive, indicating increase in salinity ($dS > 0$) and TA ($dTA > 0$), or negative, indicating a decrease in salinity ($dS < 0$) and TA ($TA < 0$). Null values of dS indicate that the surface salinity remained constant between the two occupations of one particular station. The plot of all values of (dS, dTA) reveals a linear relationship between the two variables ($n = 27$, $r^2 = 0.86$, $p < 0.01$; Fig. 4), and the slope represents the change in TA due to the change in salinity with a standard error of 4.7 μmol kg^{-1}. We computed the ratio between DIC and TA for the monthly mean surface concentrations and multiplied this ratio by the expected change in TA due to the change in salinity, to obtain the change in DIC due to the addition (or removal) of freshwater.

The contribution from river runoff was incorporated in the freshwater addition or removal term; the computation of the change in DIC (and TA) due to freshwater is based on changes in surface salinity and, therefore, implicitly includes contributions from both sea-ice and runoff. A linear regression of DIC (and TA) vs. salinity (*see* Fig. 5) yields y-intercepts, or zero-salinity end-members of DIC($S = 0$) = 649 μmol kg^{-1} and TA($S = 0$) = 797 μmol kg^{-1}, much smaller than the concentrations of samples collected in the Mackenzie River in July: DIC(Mackenzie) = 1786 μmol kg^{-1} and TA(Mackenzie) = 1880 μmol kg^{-1}. The DIC and TA concentration in sea-ice, however, ranges from 300 μmol kg^{-1} to 600 μmol kg^{-1}, indicating a stronger contribution from sea-ice melt than from runoff.

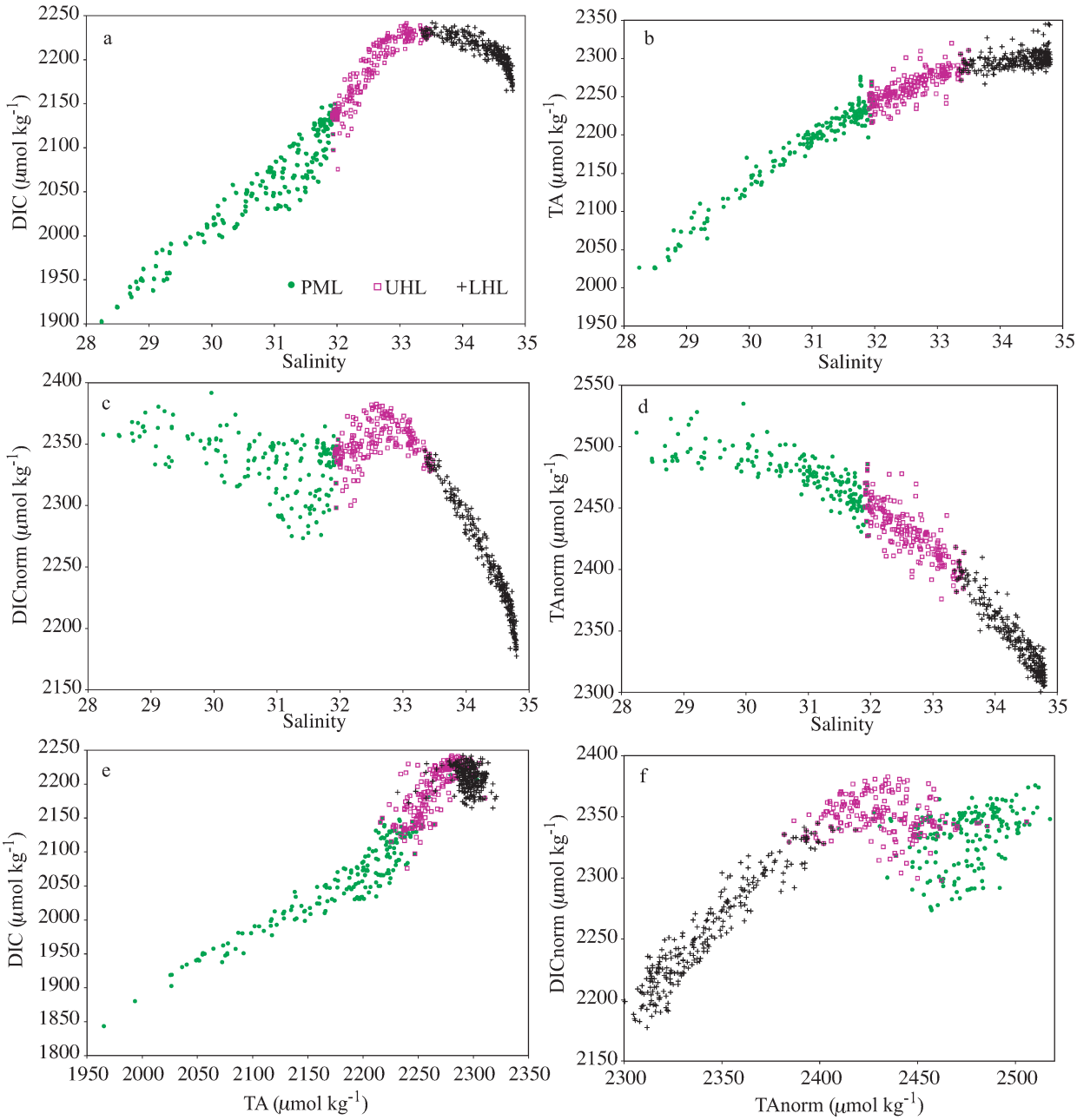

Fig. 5. The relationship between (a) DIC and salinity, (b) TA and salinity, (c) DIC_{norm} and salinity, (d) TA_{norm} and salinity, (e) DIC and TA, and (f) DIC_{norm} and TA_{norm} with the three water masses indicated. A salinity of 35 was used in the normalization. Linear regression of DIC and TA with salinity reveals the y-intercepts, or zero-salinity end members with DIC(S = 0) = 649 μmol kg^{-1} (n = 300, r^2 = 0.7), and TA(S = 0) = 797 μmol kg^{-1} (n = 300, r^2 = 0.7).

Air–sea CO_2 flux—The air–sea CO_2 flux, F_{CO_2} (mol C m^{-2} month^{-1}), was computed using the following equation:

$$F_{CO_2} = k\alpha\Delta pCO_2 \quad (1)$$

where k (cm h^{-1}) is the gas transfer velocity, parameterized as a function of the Schmidt number of the gas and the wind speed, α is the in situ CO_2 solubility (Weiss et al. 1982), and ΔpCO_2 (Pa) is the gradient in pCO_2 between the ocean and the atmosphere, as measured by the underway and foredeck systems. The gas transfer velocity, k, was computed using, hourly winds from Sachs Harbor and the formulation of Wanninkhof (1992) for short-term winds. A positive flux implies a transfer from the atmosphere into the ocean. The hourly fluxes were averaged spatially over the area of the surface box and integrated over 1 month, representing the monthly change in DIC due to the air–sea exchange of CO_2.

The CO_2 fluxes were computed assuming ice-free conditions and then scaled using a multiplier equal to 100% minus the percentage ice cover following Bates (2006) and Mucci et al. (2010; *see* Table 1). This method assumes

Table 1. Monthly estimates of percentage ice cover, estimated from Canadian Ice Service images for September 2007 through August 2008 in the budgeting area in Amundsen Gulf.

Month	J	F	M	A	M	J	J	A	S	O	N	D
% ice-cover	100	100	100	100	80	10	0	0	10	20	90	100

that sea-ice is an effective barrier to air–sea gas exchange, and that the resulting air–sea fluxes of CO_2 are a linear function of sea-ice cover. Several recent studies have suggested that sea-ice does not fully inhibit air–sea exchange of biogenic gases (e.g., Semiletov et al. 2004; Loose et al. 2009). However, the mechanisms controlling the CO_2 transfer through sea-ice likely differ from those controlling air–sea gas exchange and have not yet been adequately parameterized. Sea-ice cover was estimated using monthly ice cover images from the Canadian Ice Service.

Diffusion—The (vertical) diffusive fluxes of DIC and TA from the subsurface box into the surface box, were computed using the following equation:

$$F_d = K_v \frac{dDIC}{dz} \rho \quad (2)$$

where F_d (μmol m^{-2} s^{-1}) is the diffusive flux, K_v (m^2 s^{-1}) is the coefficient of vertical diffusion, dDIC/dz (μmol kg^{-1} m^{-1}) is the vertical gradient of DIC at the boundary between the surface and subsurface layer, and ρ (kg m^{-3}) is the water density. Several estimates of vertical diffusion in the Arctic region have been made (Munk 1966; Rudels et al. 1996; Meincke et al. 1997). We used a constant value, ($K_v = 1.1 \times 10^{-6}$ m^2 s^{-1}), from Rudels et al. (1996).

Biological processes—The net effect of biological processes on the monthly variation in DIC in the surface layer was estimated from the difference between the total observed change (ΔDIC_{obs}) and the sum of the changes due to: freshwater (ΔDIC_{fw}), air–sea CO_2 flux (ΔDIC_{as}), and vertical diffusion (ΔDIC_{vd}):

$$\Delta DIC^{s}_{bio} = \Delta DIC_{obs} - (\Delta DIC_{fw} + \Delta DIC_{as} + \Delta DIC_{vd}) + \psi_s \quad (3)$$

The last term on the right-hand side, ψ_s, represents the error, with the subscript 's' indicating the surface layer. The term includes the uncertainty associated with each of the terms in Eq. 3. The net effect of biological processes was similarly estimated for the subsurface box, excluding the effects of freshwater and air–sea exchange, but including advection (ΔDIC_{adv}):

$$\Delta DIC^{d}_{bio} = \Delta DIC_{obs} - (\Delta DIC_{adv} + \Delta DIC_{vd}) + \psi_d \quad (4)$$

with ψ_d representing the uncertainty, and the subscript 'd' referring to the subsurface layer. The resulting ΔDIC_{bio} terms account for the effect of photosynthesis and respiration including contributions from the remineralization of DOC (*see Dissolved organic carbon*), the formation and dissolution of biogenic calcium carbonate ($CaCO_3$) and, in the case of the subsurface box, exchanges of carbon with the sediments. The particulate organic carbon (POC) flux in a nearshore region of the neighboring Franklin Bay is 6.8 g C m^{-2} yr^{-1} at a depth of 200 m (Forest et al. 2008). Estimates of primary production in the Amundsen Gulf region range from 90 g C m^{-2} yr^{-1} to 175 g C m^{-2} yr^{-1} (Arrigo and van Dijken 2004); the POC flux at 200 m ranges between 4% and 8% of the primary production. Carbon losses due to burial in the sediments, at a depth of 350–380 m, thus account for a small percentage of primary production, and were assumed negligible over the annual time scale of interest (Mucci et al. 2008). Furthermore, it has been shown that sedimentation rates in Amundsen Gulf are very low (Macdonald et al. 1998; Richerol et al. 2008). Respiration of organic matter in the surface sediments is considered a source of DIC and TA to the overlying water (Fennel et al. 2008; Thomas et al. 2009); this possible contribution to the subsurface DIC (and TA) budget was neglected. The biological contribution to the monthly changes in TA, in both the surface and subsurface layers, was computed with the following equations:

$$\Delta TA^{s}_{bio} = \Delta TA_{obs} - (\Delta TA_{fw} + \Delta TA_{vd}) + \chi_s \quad (5)$$

$$\Delta TA^{d}_{bio} = \Delta TA_{obs} - (\Delta TA_{adv} + \Delta TA_{vd}) + \chi_d \quad (6)$$

where χ_s and χ_d represent the uncertainty for the surface and subsurface layer, respectively, as described above.

Error estimation—The uncertainty associated with the observed monthly changes in DIC and TA (i.e., ΔDIC_{obs} and ΔTA_{obs}) ranges from 2 μmol kg^{-1} to 3 μmol kg^{-1} in line with the uncertainty associated with the DIC and TA measurements. Nevertheless, averaging within the budgeting area may increase the uncertainty associated with the observed monthly changes. The uncertainty associated with the freshwater term is estimated from the standard error in the computation of dTA from dS (*see* Fig. 4 and *Freshwater*) and is roughly 5 μmol kg^{-1}. However, because changes in TA may be independent of salinity (i.e., nutrient uptake or regeneration during biological production or respiration), the standard error in the relationship between dTA and dS should be considered a lower limit on the uncertainty associated with changes in DIC due to freshwater inputs (ΔDIC_{fw}). The uncertainty associated with the air–sea flux term is relatively high (20%, or roughly 1.5 μmol kg^{-1}) and is largely due to uncertainty in the parameterization of the gas transfer velocity (*see* Eq. 1 [Naegler et al. 2006; Sweeney et al. 2007; Watson et al. 2009]). The uncertainty associated with the vertical diffusion term is quite high (100%), reflecting the range in estimates of K_v, but the contribution from vertical diffusion is small, resulting in an error of < 2 μmol kg^{-1}. The uncertainty associated with the horizontal advection term is also large (50%, or roughly 1 μmol kg^{-1}) due to the large error reported by Lanos (2009) on the annual mean water transports in Amundsen Gulf. Propagation of the above uncertainties results in an uncertainty for the (computed) surface ΔDIC^{s}_{bio} term of roughly 6 μmol kg^{-1}, and for the subsurface ΔDIC^{d}_{bio} of roughly 3 μmol kg^{-1}.

Table 2. Estimates of the uncertainty associated with the monthly computation of surface and subsurface values of ΔDIC_{bio} (ψ_s and ψ_d) and ΔTA_{bio} (χ_s and χ_d) and the surface value of ΔDOC_{bio} (ε_s) using a depth of 50 m for the surface layer and 250 m for the subsurface layer (*see* also Eqs. 3–7).

Term	Error [μmol kg^{-1} month^{-1} (mol m^{-2} month^{-1})]
ψ_s	9.0(0.5)
ψ_d	1.0(0.3)
χ_s	11.0(0.6)
χ_d	1.0(0.3)
ε_s	1.0(0.5)

The resulting uncertainty in the ΔTA^{s}_{bio} term is roughly 6 μmol kg^{-1}.

We estimated ψ and χ by means of Monte Carlo simulations of ΔDIC_{bio} and ΔTA_{bio}, and assumed that the standard deviations of the simulated series yield reasonable estimates of ψ and χ. The inputs for the simulation were randomly generated from distributions that most closely match the data; 10,000 points were chosen randomly for each of the model variables (i.e., each of the terms on the right-hand sides of Eqs. 3–6), using a random number generator. Following a test for normality and uniformity, the observed monthly changes, and the changes due to freshwater were represented by normal distributions. A uniform distribution was used to represent the air–sea flux, vertical diffusion, and advection terms. The uniform distribution requires the maximum value, while the normal distribution requires the mean and standard deviation; these values were taken from the monthly values of each of the terms on the right hand sides of Eqs. 3–6. For example, the following equation was used to compute the uncertainty associated with ΔDIC^{s}_{bio}:

$$\psi_s = M_{obs} - M_{fw} - M_{as} - M_{vd} \quad (7)$$

where 'M' indicates the randomly generated series. The equation was solved 10,000 times, and the standard deviation used as the magnitude of ψ_s. The resulting uncertainties associated with the surface and subsurface estimates of ΔDIC_{bio} and ΔTA_{bio} are summarized in Table 2.

Dissolved organic carbon—The observed, monthly changes in DOC were computed analogously to changes in DIC and TA using the method described in *Observed monthly changes*. Mixed-layer DOC concentrations are influenced by the addition and removal of freshwater. As discussed in *Freshwater*, the freshwater input to Amundsen Gulf is dominated by the formation and melting of sea-ice. The salinity-dependent changes in DOC were computed by multiplying the monthly value of ΔDIC_{fw} by the ratio of DOC : DIC in sea-ice (melting), or by the monthly ratio of DOC : DIC in the surface waters (sea-ice formation). A constant value of DIC in sea-ice (350 μmol kg^{-1}) was computed from the mean of all bottom 10-cm ice samples (*see Sampling and analytical measurements*). A constant value of DOC in sea-ice (64 μmol kg^{-1}), the average value of samples measured in February and March in the same region by Riedel et al. (2008), was used. These measurements reflect bottom-ice DOC concentration, and may potentially overestimate DOC in ice melt. The diffusive fluxes, from the surface to the subsurface box, were computed via Eq. 2 as described in *Diffusion*.

DOC is produced by a host of biological processes, including excretion by zooplankton, direct release by phytoplankton, and the lysis of algal or bacterial cells. This DOC may be mixed downward, or remineralized to inorganic carbon, potentially making a positive contribution to biologically mediated changes in surface DIC (i.e., $\Delta DIC_{bio} > 0$). In the subsurface waters, labile DOC is remineralized, while biologically refractory material may accumulate (Hansell and Carlson 2001).

A similar approach to that described above was used to compute the change in mixed-layer DOC due to biological processes using the following equation:

$$\Delta DOC^{s}_{bio} = \Delta DOC_{obs} - (\Delta DOC_{fw} + \Delta DOC_{vd}) + \varepsilon_s \quad (8)$$

where ε_s is the uncertainty. We estimated ε_s via the Monte Carlo simulation described in *Error estimation*, and the value is given in Table 2.

Results

The relationships between DIC and salinity, and TA and salinity, for the study area are shown in Fig. 5. In the upper 50 m of the water column, the salinity in the PML ranged from roughly 28 to greater than 31. Over the same depth range, the minimum DIC and TA concentrations were roughly 1900 μmol kg^{-1} and 2000 μmol kg^{-1} respectively, and the maximum DIC and TA concentrations (in the PML) were roughly 2150 μmol kg^{-1} and 2250 μmol kg^{-1}, respectively. Beneath the PML, the salinity range in the UHL extended from roughly 32 to 33.5. In this Pacific-origin layer, the maximum water column DIC concentrations of 2240 μmol kg^{-1} were observed. In the UHL, TA ranged from 2240 μmol kg^{-1} to 2290 μmol kg^{-1}. The deepest waters were comprised of Atlantic-origin LHL waters and the salinity ranged from 33.5 to 35. The maximum TA concentration (2305 μmol kg^{-1}) was coincident with the salinity maximum. DIC concentrations ranged from 2230 μmol kg^{-1} (at S = 33.5) to 2165 μmol kg^{-1} at S = 35. TA displayed nearly conservative behavior with the slope of the linear relationship between TA and salinity changing with respect to the water mass. The relationship between DIC and salinity, on the other hand, was nearly conservative within the PML, and nonconservative in the deeper water column, implying the dominance of a process other than mixing between the UHL and LHL waters. The nonlinear, or bow-shaped, relationship between DIC and salinity in the UHL and LHL waters will be explored in more detail (*see Nutrient uptake and net community production*).

The relationship between salinity-normalized DIC (DIC_{norm} = 35DIC/S) and salinity is shown in Fig. 5c and the relationship between salinity-normalized TA (TA_{norm} = 35TA/S) and salinity is shown in Fig. 5d. The normalization of DIC (and TA) to a constant salinity removes the effect of freshwater inputs from the measured

concentrations. Variability in the salinity-normalized concentrations are, thus, primarily controlled by water temperature (i.e., by the solubility of CO_2), biological processes, air–sea exchange of CO_2, and mixing of water masses. The relationship between DIC_{norm} and salinity (Fig. 5c) indicates that biology dominates at low salinity ($S < 32$, the upper 50 m of the water column, or the PML). Additional influences of mixing and air–sea exchange, with a relatively small range of DIC_{norm} from roughly 2300 μmol kg^{-1} to 2350 μmol kg^{-1} also occur over this salinity (and depth) range. In the subsurface layer, mixing and biological processes dominate over the salinity range of $32 < S < 35$ with DIC_{norm} ranging from a maximum of roughly 2300 μmol kg^{-1} (near $S = 32$) and a minimum of 2175 μmol kg^{-1} at salinities of roughly 35 (*see Nutrient uptake and net community production*).

The relationship between DIC and TA is shown in Fig. 5e. The ratio between DIC and TA is roughly 1 : 1 in the PML. This ratio increases to 1.2 : 1 in the UHL; respiration, or the remineralization of organic matter produced in the surface layer, or PML, occurs primarily in the UHL, increasing DIC and also the ratio of DIC : TA. In the LHL, the TA continues to increase (relative to the PML and UHL) primarily as a function of increasing salinity. DIC in the LHL is reduced, relative to the UHL due to the reduction of respiration, or remineralization of organic matter, as a function of depth. The Pacific-origin UHL waters have the highest concentrations of DIC, while the most saline Atlantic-origin LHL waters have the highest concentration of TA with lower DIC relative to the UHL. The relationship between DIC_{norm} and TA_{norm} is shown in Fig. 5f. With the effect of freshwater addition and removal accounted for in the observed concentrations, biological processes dominate in the PML while the lower water column is dominated by mixing, indicated by the nearly 1 : 1 relationship between DIC_{norm} and TA_{norm} in the LHL and UHL.

Annual cycles—The annual cycles of water column salinity, temperature, DIC, TA, pCO_2, pH, Ω_{Ar}, and the Revelle Factor are plotted in Fig. 6. The water temperature (*see* Fig. 6b) was relatively homogeneous both with depth and throughout the year, with values ranging from roughly −1.5°C to 1.5°C. During the brief summer season ice retreat allowed a warming of the near-surface waters to 7°C or 8°C. In the salinity profile (Fig. 6a), the effect of sea-ice formation and melt was clearly seen in the upper (PML) water column. Below the PML is the Pacific-origin upper halocline layer (UHL) that overlies the more saline Atlantic water mass. This structure is also reflected in the DIC profile (*see* Fig. 6c), where lower concentrations, with large seasonal variations, were seen at the surface, due both to the input and removal of freshwater, and to the carbon draw-down by photosynthesis. High DIC concentrations in the UHL result from the export and remineralization of organic matter from the surface layer (*see* Fig. 5a,e), and also reflect the presence of older Pacific source-water in this layer. Maximum values of pCO_2, and minimum values of pH and Ω_{Ar}, are also found within this depth range (Fig. 6d–f). Conditions of aragonite undersaturation (i.e., $\Omega_{Ar} < 1$) were observed in the UHL between depths of roughly 50 m and 150 m. This undersaturation is due to the remineralization of organic matter, which increases the concentration of DIC and raises the pCO_2, lowering pH and Ω_{Ar} (*see* Fig. 6e–f). Below a depth of roughly 150 m, conditions of weak aragonite saturation were observed (*see* Fig. 6g). The seasonal changes in TA (Fig. 6d), generally followed the same surface patterns as DIC and salinity. The formation and melting of sea-ice exerts a significant control on surface concentrations of both DIC and TA. Unlike river water, which adds freshwater as well as relatively high concentrations of DIC and TA (on the order of 1800 μmol kg^{-1}) to the system, sea-ice melt-water contains much lower concentrations of DIC and TA (on the order of 300 μmol kg^{-1}) and dilutes the surface waters, reducing the concentration of DIC and TA. Conversely, the formation of sea-ice removes freshwater leaving salinity, DIC, and TA behind in a process referred to as brine rejection. Thus sea-ice formation concentrates the surface waters with respect to salinity, DIC, and TA. The rejected brine is denser than the surrounding waters and sinks; this process provides a potential export pathway for carbon from the surface waters. If the high salinity, and DIC-rich brine, sinks below the PML the carbon contained in the brine is potentially sequestered from the surface layer and from exchange with the atmosphere (Bates 2006; Bates and Mathis 2009). Changes in DIC and TA due to the melting and formation of sea-ice will be discussed in more detail in the next section.

Surface pCO_2 was undersaturated with respect to the atmosphere throughout the year within the study area. There was a decrease in pCO_2 and DIC (and an increase in pH) corresponding to the growth of under-ice algae (Riedel et al. 2006), between day of year (DOY) 100 and DOY 150, before the onset of sea-ice melt following DOY 150. The growth of phytoplankton in sea-ice decreases the pCO_2 by consuming DIC. The DIC concentration in the bottom 10 cm of ice decreased from 384 μmol kg^{-1} on DOY 115, to 319 μmol kg^{-1} on DOY 130 at the same station (*see* Table 3). After DOY 200, the ice began to melt and much lower concentrations of DIC in the ice (roughly 180 μmol kg^{-1}) were observed. There was an increase in pCO_2 and decrease in pH in the surface waters following DOY 200, after the ice had begun to melt, and the summer phytoplankton bloom had depleted the surface-water DIC. The open-water bloom coincided with the peak Mackenzie River discharge to the region. The Mackenzie River has relatively high DIC (1786 μmol kg^{-1}) and TA (1880 μmol kg^{-1}) concentrations (measured in Jul 2008), as well as a large pool of POC (Macdonald et al. 1987). With a pCO_2 of roughly 700×10^{-1} Pa, runoff from the Mackenzie River is supersaturated with respect to the atmosphere (Vallières et al. 2008). However, we detected only a very small contribution of runoff from the Mackenzie River in Amundsen Gulf. This short-lived increase in pCO_2, and corresponding decrease in pH is rather the result of the brief summer warming of the surface waters (Fig. 6b). The thermodynamic effect of temperature on seawater pCO_2 results in a pCO_2 increase of roughly 4% for each 1°C increase in temperature (Takahashi et al.

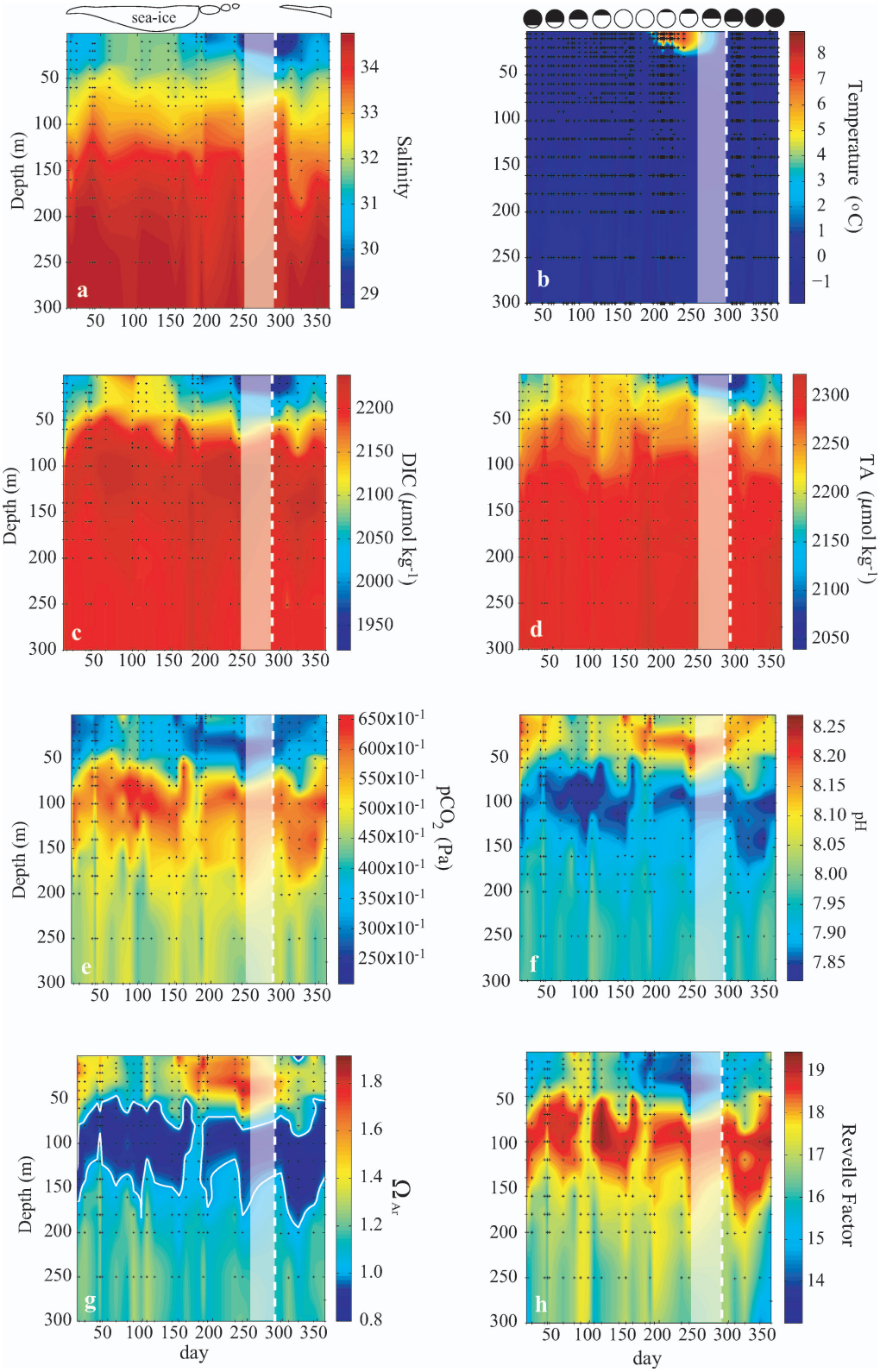

Fig. 6. Temporal evolution of (a) temperature, (b) salinity, (c) DIC, (d) TA, (e) pCO_2, (f) pH, (g) Ω_{Ar} (with the contour line indicating $\Omega_{Ar} = 1.0$), and (h) the Revelle factor in Amundsen Gulf. The data to the right of the vertical white dashed line are from October through December 2007, while the data to the left of this line are from January to August 2008. The data within the white shaded area are an interpolation between August 2008 and October 2007. The annual cycle of sea-ice cover and sunlight are shown schematically above panels a and b, respectively.

Table 3. Concentrations of dissolved inorganic carbon (DIC; μmol kg^{-1}) measured in the bottom 10 cm of ice and the corresponding salinity (S). The growth of under-ice algae after day of year (DOY) 115 decreases the concentration of DIC.

DOY	Station position	DIC	S
17	71.5°N, 125.7°W	393	5.1
23	71.4°N, 125.4°W	404	5.8
115	70.5°N, 122.4°W	384	5.1
126	70.5°N, 122.4°W	356	5.5
130	70.5°N, 122.4°W	319	3.9

2002). The warming of the surface waters from 1°C to 8°C would increase pCO_2 by roughly 90×10^{-1} Pa (with an initial value of 325×10^{-1} Pa). Over the same period one would expect a corresponding decrease in surface-water Ω_{Ar}; however, this parameter is less sensitve to changes in temperature than pCO_2 and pH and the decrease is undetected within Fig. 8g.

Seasonal profiles from repeated (Oct, Feb, May, and Jul), occupations of the same station (indicated by the star in Fig. 2) are presented in Fig. 7. Each of these profiles are mean values generated from between 2 and 4 occupations of the station within a given season. Subsurface salinity and DIC and TA concentrations were fairly constant throughout the year, whereas the surface DIC concentrations ranged from 2125 μmol kg^{-1} in winter to 1934 μmol kg^{-1} in autumn. Sea-ice covered the water in both winter and spring, and the salinity profiles showed stable surface stratification and a well-developed PML in the upper 50 m. The winter profiles of salinity and TA indicated near-uniform concentrations from the surface to a depth of roughly 40 m. In the transition from winter to spring there was a salinity increase from $\sim$ 31.5 to 32 (Fig. 7a). Over the same period the surface DIC concentration decreased (Fig. 7b). An increase in salinity, if it was the only process acting on DIC, would result in an addition of DIC to the surface waters, and the DIC profile would resemble the upper portion of the TA profile in spring (Fig. 7). The observed change in DIC between winter and spring was, thus, the result of biological uptake by under-ice algae, which was confirmed by a coincident increase in dissolved oxygen (not shown), and the accumulation of DOC in the bottom ice (Riedel et al. 2008).

If we suppose that the winter-to-spring transition comprises only salinity-dependent changes in DIC, we can compute a profile of expected spring DIC concentration (DIC_{ex}) based on the change in salinity between winter and spring (Fig. 7b inset). The DIC_{ex} profile would represent the spring DIC concentrations resulting from changes in salinity alone. If we compare this computed profile with the in situ DIC profile from spring in the surface mixed-layer, we see that the in situ spring concentrations were much lower than predicted by the change in salinity. As discussed above, this decrease in DIC is attributed to the growth of under-ice algae. Integrating the difference between these two profiles over the 50-m depth range (shaded area), yields an estimate of the biologically mediated change in DIC (1.2 mol C m^{-2} month^{-1}) at this station. We compare this value to the monthly estimates of production over the same period, (1.7 mol C m^{-2} from Feb to May), in *Nutrient uptake and net community production*. The uptake of inorganic carbon by under-ice algae precedes the open-water phytoplankton bloom (Gradinger 1996; Renaud et al. 2007), the effect of which was seen in the further reduction of surface DIC between spring and summer. Both summer and autumn DIC data reflect open-water conditions and the reduction in salinity resulting from sea-ice melt. With the return of sunlight, the onset of (open-water) photosynthesis decreased surface DIC concentrations.

Seasonal profiles of pCO_2, pH, and Ω_{Ar} are given in Fig. 7d–f. Photosynthetic uptake of carbon by phytoplankton in the surface layer decreased DIC and pCO_2, while increasing pH and Ω_{Ar}. The effect of biological activity between winter and summer can also be seen in the pCO_2 profiles, which showed a reduction from winter through spring and into summer; pH and Ω_{Ar} both increased over the same period. In the subsurface waters, respiration, or remineralization of organic matter, increased DIC and pCO_2, while pH and Ω_{Ar} were depressed. Accordingly, between spring and summer, below a depth of roughly 50 m, DIC increased (Fig. 7b), and both pH and Ω_{Ar} decreased (Fig. 7e,f). Between summer and autumn the largest decrease in surface DIC was observed, coincident with the largest decrease in surface salinity (from roughly 31.2 to 28.7). Surface pCO_2 also decreased, while there was an increase in Ω_{Ar} over the same period. In the Amundsen Gulf region, changes in salinity are attributed to both runoff and sea-ice melt and formation (*see Freshwater*); Ω_{Ar} has been shown to decrease with increasing sea-ice melt water (Bates et al. 2009; Chierici and Fransson 2009), as observed in the summer-to-autumn transition (Fig. 7f). The autumn DIC, TA, and pCO_2 minima result from the dilution of the mixed-layer by sea-ice melt-water, resulting in a decreased Ω_{Ar}, unbuffered by photosynthetic CO_2 uptake seen during the winter–spring and spring–summer transitions.

It should be noted that the above discussion regarding summer-to-autumn transitions, which will be revisited in the following section, is based on data collected in two different years. Hence, we assumed that interannual variability does not compromise the reconstruction of the annual cycle using data from October 2007 through August 2008.

Processes controlling variability of DIC and TA—Results of the mass balance computations (*see* Eqs. 3–6) are shown in Fig. 8. The observed, monthly mean changes in surface DIC and TA (Fig. 8a,b) range from -60 μmol kg^{-1} to 60 μmol kg^{-1}, and are mainly dominated by changes due to freshwater inputs and biological processes. From March to October, contributions from sea-ice melt decreased surface DIC and TA concentrations; from November to February the formation of sea-ice and corresponding brine rejection increased surface concentrations of DIC and TA. The largest positive changes in DIC due to freshwater fluxes occurred in March and December and were associated with sea-ice formation; the largest negative changes in DIC due to freshwater fluxes were observed in June and October and

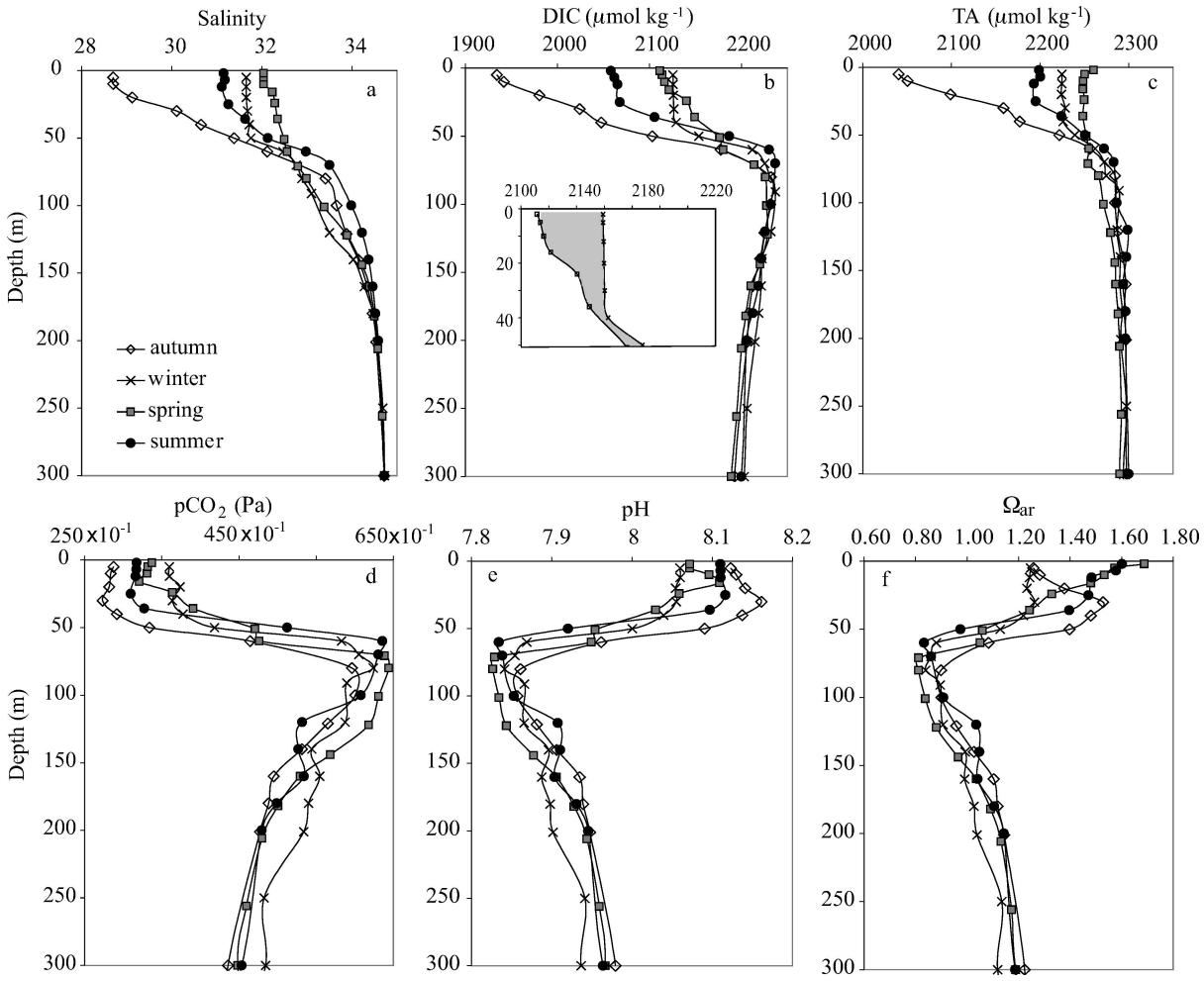

Fig. 7. Seasonal profiles of (a) salinity, (b) DIC, (c) TA, (d) pCO_2 (e) pH, and (f) Ω_{Ar} generated from repeated sampling at the same station (*see* Fig. 2 for station location). Inset: the in situ winter DIC profile in the upper 50 m is given by the x's, and the expected spring DIC profile computed from the winter-to-spring salinity change is given by the open squares.

resulted from sea-ice melt, with additional contributions from river runoff in late June and early July.

Lateral advection and vertical diffusion played a minor role with respect to surface changes in both DIC and TA. The surface waters of Amundsen Gulf were weakly undersaturated with respect to atmospheric CO_2 throughout the year. Hence, during the open-water months, the region acted as a moderate sink for atmospheric CO_2, as reported by Mucci et al. (2010), but these inputs made only a minor contribution to the monthly changes in surface DIC. Biological processes thus made up the balance of the observed monthly changes in surface DIC and TA. Photosynthesis decreased surface DIC concentrations by roughly 20 μmol kg^{-1} month^{-1} from April through July, and biological processes made a modest contribution to changes in DIC during the remainder of the year, with increases in DIC due to respiration in the surface waters occurring in December and January.

The effect of biological activity on surface TA was small (Fig. 8b), with small increases in July and August corresponding to nutrient assimilation (and decreases in NO_3^- during photosynthesis), while the negative values in September through December corresponded to the regeneration of nutrients (and increases in NO_3^-) through respiration. There is no evidence that the negative values of ΔTA_{bio} in April and May, and the positive value of ΔTA_{bio} in January were the result of the respective formation (in spring) and dissolution (in winter) of $CaCO_3$, despite the correspondence with changes in DIC. As shown in Fig. 8b, the primary control on TA is freshwater input, and any other effects are minor. The reliable quantification of these minor processes, however, goes beyond the limits of our method.

The observed monthly changes in subsurface DIC (Fig. 8c) were more modest than those in the surface waters. Lateral advection reduced DIC, with lower inorganic carbon waters from the east flowing into Amundsen Gulf throughout the year. The contribution from vertical diffusion, represented by a loss of higher inorganic carbon water to the surface layer was near zero, when integrated over the large volume of the subsurface layer. Respiration, fueled by the delivery of organic matter

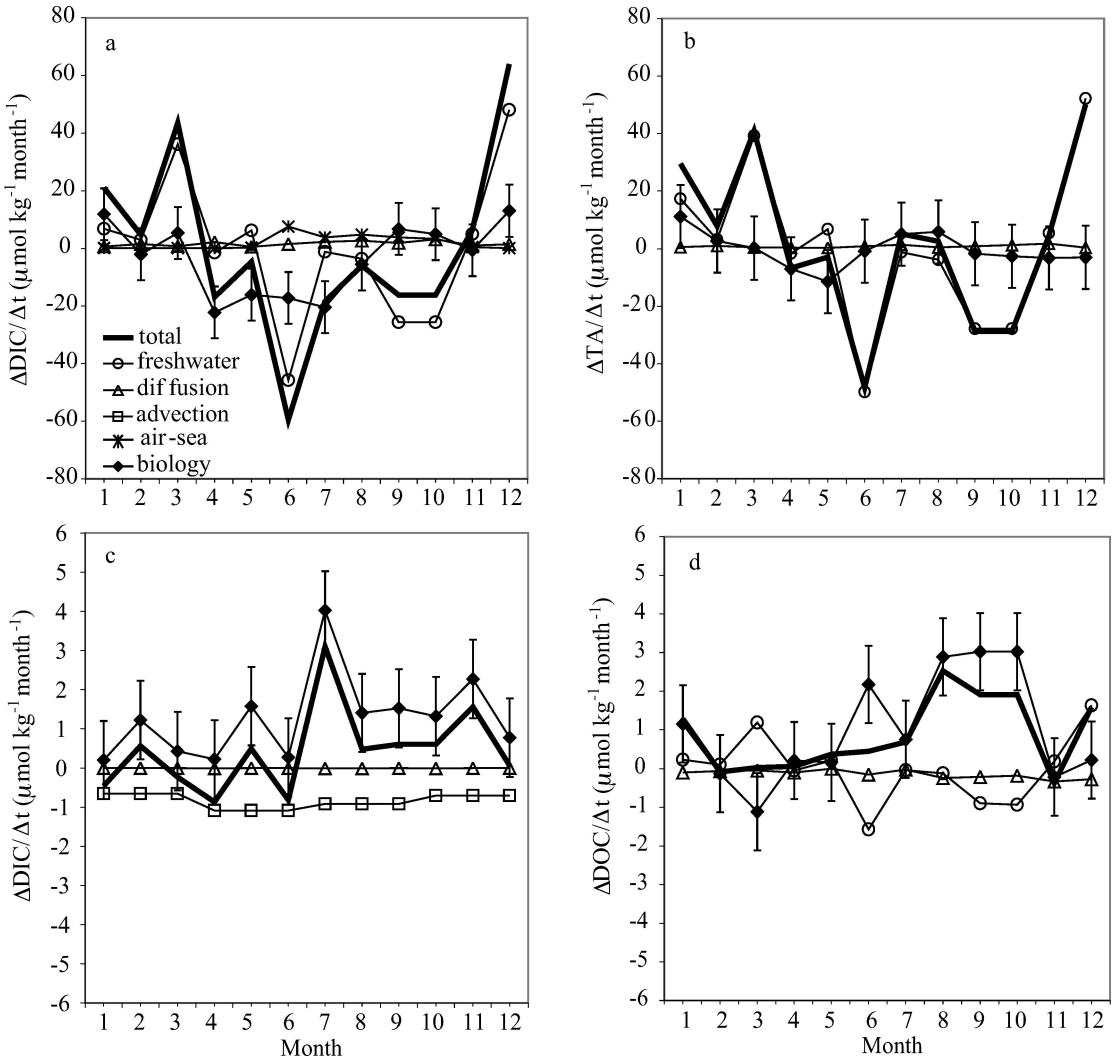

Fig. 8. Controls on (a) surface DIC, (b) surface TA, (c) subsurface DIC, and (d) surface DOC. The surface extends from 0 m to 50 m, and the subsurface from 50 m to 300 m. Please note that the October through December values are based on samples collected in 2007, while the January through August values are based on samples collected in 2008. The September values are the mean of the computed monthly concentrations from August and October.

produced in the surface, was ongoing throughout the year, as supported by the positive values of ΔDIC_{bio} (Fig. 8c). The maximum change in subsurface DIC due to biological activity takes place in July, roughly 1 month out of phase with the maximum surface production.

Results of the surface DOC mass balance computation (Eq. 12) are shown in Fig. 8d. Changes due to freshwater inputs mirror those in surface DIC and TA, as described above (*see Freshwater and Dissolved organic carbon*). Advection and diffusion played only a minor role. The variations of DOC from April to October, were dominated by positive changes due to contributions from biological processes. Modest increases in mixed-layer DOC in March and April, coinciding with DIC draw-down over the same period, were followed by a more significant production of DOC in June, and from July to October. The large, significant increase in DOC attributed to biological processes in the surface layer in June was nearly the same magnitude as the subsequent late-summer production that occurred over a shorter period. This increase in DOC is attributed to the release of DOC from melting ice. There was a large (biological) accumulation of DOC in the bottom ice in spring (Riedel et al. 2008; *see Annual cycles*), which was released to the surface water upon ice-melt. Sea-ice DOC concentrations as high as 2000 μmol kg^{-1} have been measured in April and May in the Amundsen Gulf region (Riedel et al. 2008). We used a much lower, constant value (DOC_{ice} = 65 μmol kg^{-1}) to compute the ΔDOC_{fw} consistent with the method used to estimate ΔDIC_{fw} (*see Freshwater and Dissolved organic carbon*). Hence the addition of sea-ice melt water resulted in a dilution of DOC, and was attributed in spring and summer to biology. The postbloom increase in DOC, from July to October, was likely associated with both ice-melt, and nutrient-limited conditions. In the latter case, DOC was produced from the consumption of DIC in the absence of nitrate, and by the degradation of (recently produced) organic matter.

Atmospheric CO_2 uptake—The monthly integrated air–sea CO_2 fluxes are plotted in Fig. 9. The surface waters in Amundsen Gulf were undersaturated with respect to atmospheric CO_2 throughout the year. As described in the Methods section, the air–sea fluxes were scaled to account for ice-cover in the region because it is assumed to inhibit gas transfer between the ocean and the atmosphere. Both the uncorrected and the ice-cover corrected fluxes are shown in Fig. 9. A large gradient in pCO_2 drove the strong (uncorrected) fluxes seen from January to May. The ice began to melt in June and decreased surface-water pCO_2, increasing the ΔpCO_2. The water warms through the summer and the lowered CO_2 solubility counteracts the uptake of DIC by phytoplankton. With ice formation in November and December, the ice-cover corrected fluxes are diminished despite the persistence of a strong air–sea gradient in pCO_2. We estimate that the annual uptake of CO_2 in Amundsen Gulf is $F_{CO_2} = 1.2$ mol C m^{-2} yr^{-1}. If ice-atmosphere CO_2 fluxes prove significant, then the method used to scale the fluxes under conditions of ice-cover may result in an underestimate of the Amundsen Gulf sink for CO_2 on the annual scale. Nevertheless, at this time reliable parameterization for gas fluxes between the ocean and the ice are lacking. Furthermore, the role of sea-ice as an inter-facial medium between the ocean and the atmosphere is not well-constrained. The method used here reflects the state of available knowledge, and estimates can be considered a lower limit on the annual air–sea CO_2 flux.

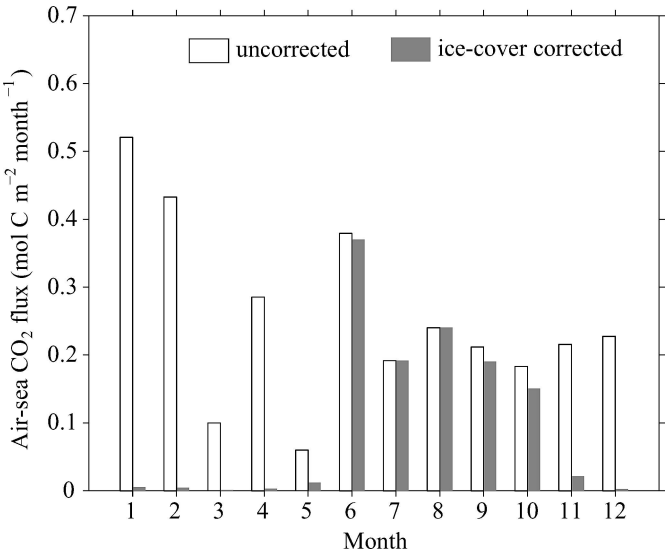

Fig. 9. The monthly air–sea CO_2 fluxes in Amundsen Gulf, with positive values indicating a transfer from the atmosphere to the ocean. The white bars are the uncorrected fluxes, computed without taking ice-cover into account. The gray bars are the ice-cover corrected fluxes (*see* Table 2). The region acts as a sink for atmospheric CO_2 throughout the year. The annual (ice-corrected) flux is F_{CO_2} =1.2 mol C m^{-2} yr^{-1}, the annual uncorrected flux would be $\bar{F} = 3.0$ mol C m^{-2} yr^{-1}.

Discussion

Nutrient uptake and net community production—Net community production (NCP) is the difference between net primary production (NPP) and heterotrophic respiration (R). The latter can, therefore, be related to biologically mediated changes in DIC:

$$NCP = NPP - R = -\Delta DIC_{bio} \quad (9)$$

NCP is commonly computed from nitrate or phosphate uptake and converted to carbon units using the conventional Redfield ratio of C : N : P = 106 : 16 : 1. This method is reliable when nitrate and phosphate are not depleted, and DIC, nitrate, and phosphate are taken up in Redfield proportions (Arrigo 2005; Bozec et al. 2006). However, DIC may still be consumed when nutrients are depleted, and carbon-based estimates of NCP often exceed nitrogen-based estimates (Thomas et al. 1999; Bozec et al. 2006; Tremblay et al. 2008).

Monthly values of ΔDIC_{bio}, ΔNO_3^-, ΔSi, and the ratios of $\Delta DIC{:}\Delta NO_3^-$, and $\Delta Si{:}\Delta NO_3^-$ are given in Table 4. Increased consumption of silicate relative to nitrate has been linked to iron or nutrient limitation in phytoplankton (Hutchins and Bruland 1998; Takeda 1998). The southern Beaufort Sea is nitrate-limited after sea-ice break-up and the onset of the spring and summer phytoplankton blooms (Tremblay et al. 2008). However, NCP can be sustained upon nitrate depletion by regenerated nitrogen, nitrogen fixation, or by an allocthonous nitrogen source. From April to June, DIC and NO_3^- were taken up in roughly Redfield proportions, with the mean value of $\Delta DIC : \Delta NO_3^- = 6.2$ over this period. In April, the $\Delta Si : \Delta NO_3^-$ was near unity, but increased significantly in May and June, indicating nutrient limitation most likely attributable to a nitrate depletion in the surface layer. The under-ice algae are likely dominated by diatom species (Horner and Schrader 1982), which may explain the ratio of $\Delta Si : \Delta NO_3^-$ at the beginning of the productive season. After the ice break-up, nutrients quickly become depleted by the open-water phytoplankton bloom, which is dominated in June and July by flagellates, explaining part of the change in $\Delta Si : \Delta NO_3^-$ over this period (Jull-Pedersen et al. 2010).

An estimate of NCP from biologically driven changes in DIC (Eq. 9) is plotted in Fig. 10. In winter, NCP was negative in the surface waters, corresponding to a positive change in DIC (respiration). From April to August, during the productive summer period, NCP was positive. The subsurface indicated a maximum respiration in July, as a result of an increased delivery of organic matter from the surface layer. Integrating the monthly values of NCP over the year yields a value of $NCP_s = 2.1 \pm 1.7$ mol C m^{-2} yr^{-1} in the surface and a respiration inventory of $R = 3.8 \pm 1.0$ mol C m^{-2} yr^{-1} in the subsurface. Integrating the monthly values of NCP from winter (Feb) to spring (May) yields a value of 1.7 mol C m^{-2} over the winter–spring transition, in good agreement with the estimate made by graphical integration (1.2 mol C m^{-2}, *see Annual cycles*). Integrating the biologically mediated changes in mixed-layer DOC, over the annual cycle yields a production of 0.61 ± 0.24 mol C m^{-2} yr^{-1}, which corresponds to 28% of NCP; this value is somewhat higher than an estimate of DOC production in the nearby Chukchi Shelf (10%;

Table 4. Monthly values of ΔDIC_{bio}, ΔNO_3^-, ΔSi, (μmol kg^{-1}), the ratios of $\Delta DIC{:}\Delta NO_3^-$, and $\Delta Si{:}\Delta NO_3^-$, NCP and air–sea CO_2 flux (F_{CO_2}, mol C m^{-2} month^{-1}), during the productive season, and the annual value of ΔDIC_{bio} (μmol kg^{-1} yr^{-1}), and annual NCP and F_{CO_2} (mol C m^{-2} yr^{-1}). In July and August, nutrients were exhausted and the carbon and nutrient ratios were, therefore, not computed. *See* also Figs. 8a, 9, and 10.

Month	ΔDIC_{bio}	ΔNO_3^-	ΔSi	$\Delta DIC{:}\Delta NO_3^-$	$\Delta Si{:}\Delta NO_3^-$	NCP	F_{CO_2}
Apr	−21.6	−3.4	−3.7	6.2	1.1	1.11	0.00
May	−16.1	−2.6	−6.6	6.2	2.5	0.81	0.01
Jun	−17.2	−1.8	−5.5	9.4	3.0	0.86	0.38
Jul	−20.4	—	—	—	—	1.02	0.19
Aug	−5.6	—	—	—	—	0.28	0.24
Annual	−42.2	—	—	—	—	2.1	1.2

Mathis et al. 2007), but in line with the estimate of Gosselin et al. (1997) for the Arctic Ocean.

We made an alternate estimate of subsurface respiration. In brief, the deviation of in situ DIC from a linear relationship between DIC and salinity indicates a nonconservative, biological process (respiration). The linear relationship between DIC and salinity is based on the two-end member mixing of Pacific- and Atlantic-origin water of salinity 33.1 and 34.8, respectively. Nonconservative variations in DIC (ΔDIC_{resp}) are expressed as the difference between the expected DIC (DIC_{ex}, resulting from idealized mixing), and the observed DIC (DIC_{obs}):

$$\Delta DIC_{resp} = DIC_{obs} - DIC_{ex} \quad (10)$$

Positive values of ΔDIC_{resp} indicate that respiration exceeds production and correspond to a surplus of inorganic carbon. Profiles of DIC_{ex} are computed from salinity data and the following relationship: $DIC_{ex} = -48.24S + 3832$. Using Eq. 10, ΔDIC_{resp} is computed for each sample. These values were then integrated over the depth range of the subsurface layer (50–300 m), and a mean value of ΔDIC_{resp} = 4.1 mol C m^{-2} was computed. Applying the residence time (18 months) of the water in the subsurface box obtained from the transport estimates of Lanos (2009), we arrive at a subsurface respiration of 2.7 mol C m^{-2} yr^{-1}, which is in agreement with the above estimate (*see* also Fig. 10).

Estimates of primary production in Amundsen Gulf range from 7 mol C m^{-2} yr^{-1} to 15 mol C m^{-2} yr^{-1} (Arrigo and van Dijken 2004). We assume that between 15% and 30% of primary production is exported from the surface layer in Amundsen Gulf, following a recent estimate of vertical export by Jull-Pedersen et al. (2010). Thus, roughly 2 mol C m^{-2} yr^{-1} POC leaves the surface layer. According to the carbon flux estimates of Forest et al. (2008), roughly 0.45 mol C m^{-2} yr^{-1} of marine POC reaches a depth below

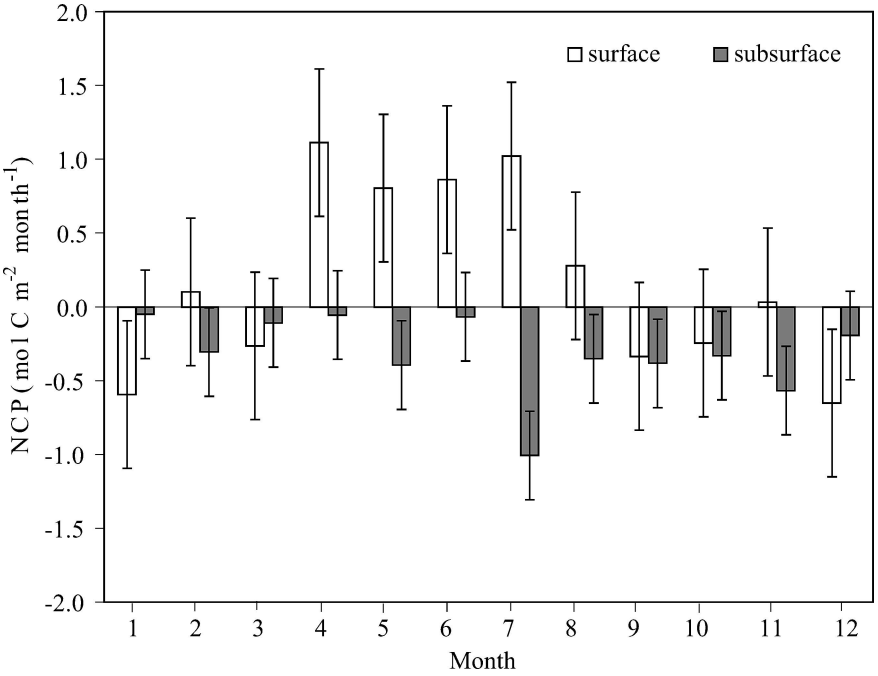

Fig. 10. Monthly values of NCP, with surface values shown in white, and subsurface values shown in gray. Error bars indicate the estimated 0.5 mol C m^{-2} month^{-1} uncertainty in the surface layer, and 0.3 mol C m^{-2} month^{-1} in the subsurface layer estimated from the Monte Carlo simulation (*see Error estimation* and Table 1).

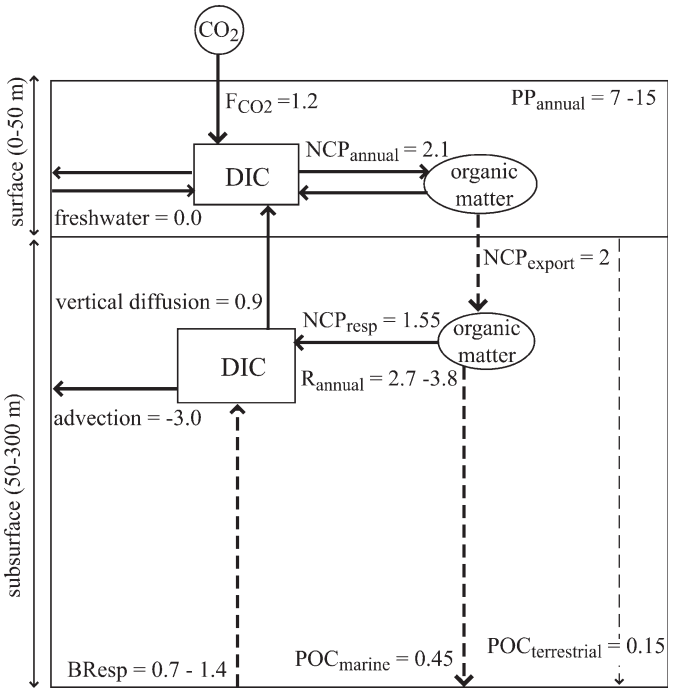

Fig. 11. A schematic representation of the inorganic carbon budget for Amundsen Gulf. All values are given in units of [mol C m^{-2} yr^{-1}]. The solid arrows indicate computations made in the current study; dashed arrows indicate values take from the literature. The surface DIC losses to NCP are balanced by atmospheric CO_2 uptake and the delivery of carbon-rich water from below. NCP is exported from the surface layer and respired in the subsurface. POC fluxes below 200 m amount to 3% to 6% of annual surface primary production (PP_{annual}), and include contributions from both marine (POC_{marine}) and terrestrial ($POC_{terrestrial}$) sources (Forest et al. 2008). Benthic respiration (BResp; Renaud et al. 2007) balances the excess carbon computed with the simple two-box model within the uncertainty of the computation (*see* Eqs. 3–6, and Fig. 3), with possible contribution from lateral advection, which cannot be accounted for with the method presented here.

200 m, with an additional contribution of 0.15 mol C m^{-2} yr^{-1} from terrestrial sources (Fig. 11). The amount of carbon available for respiration in the subsurface layer is then 1.55 mol C m^{-2} yr^{-1}. This implies that there is a subsurface carbon excess of 1.2 mol C m^{-2} yr^{-1} to 2.3 mol C m^{-2} yr^{-1}. A possible source of this excess inorganic carbon is benthic respiration, which was neglected in the subsurface DIC budget (*see Biological processes*). Using the benthic oxygen demand of Renaud et al. (2007), based on data from January to July, and assuming the mean value is valid over the whole year, and the Redfield ratio of $O_2 : CO_2 = 138 : 106$, this contribution ranges from 0.7 mol C m^{-2} yr^{-1} to 1.4 mol C m^{-2} yr^{-1} (*see* Fig. 11). It has been suggested that little, if any, sediment accumulation occurs in the Amundsen Gulf region (Richerol et al. 2008), and high turbidity above the sediment surface has been reported (Mucci et al. 2008; Magen et al. 2010). If all, or the majority of the POC flux observed was consumed by the benthic community, respiration of this organic matter could account for the excess DIC computed here, within the uncertainty of the budget computations. An alternate explanation is that the excess subsurface respiration is fueled by organic material delivered laterally to the region. This influx of particulate and, or, dissolved organic matter, is difficult to constrain using the present approach, which assumes that lateral or horizontal advection in the subsurface occurs only along the direction of the mean water flow (north–northwest) from Amundsen Gulf toward the Southern Beaufort Sea (Lanos 2009).

In autotrophic systems, such as the surface layer in Amundsen Gulf, there is a net production of organic matter at the expense of inorganic carbon and nutrients. In contrast, heterotrophic systems are defined by a net consumption of organic matter and release of inorganic carbon and nutrients. Amundsen Gulf is, therefore, overall net heterotrophic (Alonso-Sáez et al. 2008; Garneauet al. 2008), despite the autotrophy of the surface layer, which acts as a sink for atmospheric CO_2. Previous studies have indicated that stratified systems are often partitioned this way (Bozec et al. 2005; Thomas et al. 2005). The annual cycle of biologically meditated changes in surface and subsurface DIC are shown schematically in Fig. 12. In the surface layer, respiration dominated between January and March when the waters are ice-covered and the region receives very little sunlight. In April, the growth of under-ice algae reduced surface DIC (and nutrient) concentrations; production continued under the ice until June, when ice break-up gave way to the open-water phytoplankton bloom, which rapidly depleted the surface nutrients and continues to decrease surface DIC through August. A portion of the DIC lost to the production of organic matter was replaced by the uptake of atmospheric CO_2 from June through September. In October, sea-ice began to reform and the surface layer became dominated by respiration. In the subsurface layer carbon accumulated due to organic matter respiration. The delivery of heavy (diatom) under-ice algae was seen in the first of two subsurface respiration peaks in May, roughly 1 month after the onset of the under-ice bloom. The delivery of organic matter from the open-water bloom was seen in July, also about a month out of phase with the onset of the phytoplankton bloom. The subsurface peak in July was in consistent with the sediment-trap data of Forest et al. (2008), which also show an annual maximum in July. The material was exported from of the surface layer in spring and summer upon aggregation with terrigenous material that promotes sinking; this land-derived material may come from the rivers, or from the melting of land-fast sea-ice.

Surface CO_2 undersaturation—The upper 50 m of the water column in Amundsen Gulf were undersaturated with respect to atmospheric CO_2 throughout the sampling year (Fig. 6e, and air–sea CO_2 flux). The capacity of seawater to absorb CO_2 depends on its buffer capacity (Takahashi et al. 1993; Sabine et al. 2004), which is described by the Revelle factor. This factor quantifies the change in pCO_2 for a given change in DIC, and is proportional to the ratio of DIC : TA (Revelle and Suess 1957). Waters with low Revelle factor (e.g., 8–10) have a larger potential capacity to absorb anthropogenic CO_2 and vice versa (Sabine et al. 2004). Warm tropical, and subtropical, waters have

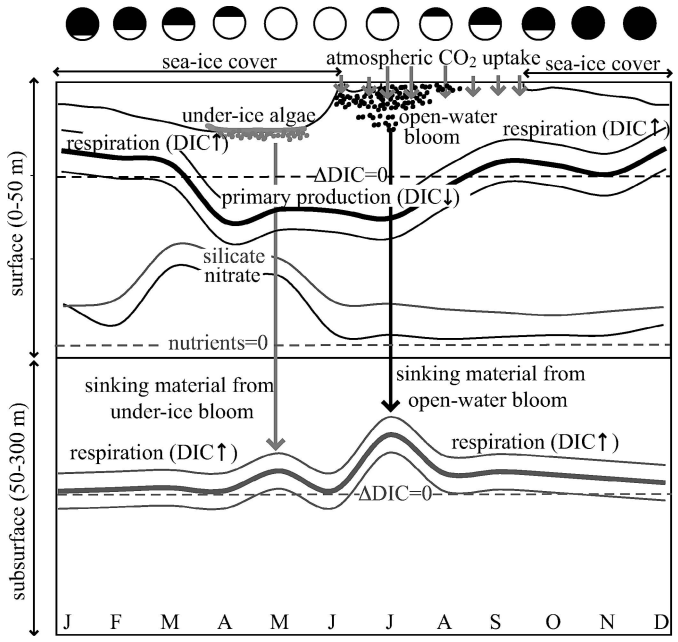

Fig. 12. The annual cycle of biologically mediated changes in DIC in the surface and subsurface layers are shown schematically. The bold and thin lines indicate the computed monthly values and the associated uncertainty, respectively (*see* Fig. 10), the dashed lines indicated $\Delta DIC_{bio} = 0$ such that positive values are associated with respiration and negative values with production. The annual cycles of surface nitrate and silicate are also shown; please note that the nutrient lines indicate concentrations and not changes, so that the dashed line indicates nutrient depletion. The sinking of organic material due to the under-ice and open-water blooms, the annual cycle of sea-ice and sunlight, and the uptake of atmospheric CO_2 during the open water season are also shown schematically.

relatively a low Revelle factor and, therefore, a large potential anthropogenic CO_2 uptake, despite the lower CO_2 solubility at high temperature, because the Revelle factor quantifies a response to a change and not the steady state of the system. High-latitude and polar oceans have relatively higher Revelle factors, and a smaller potential capacity to absorb anthropogenic CO_2 (Sabine et al. 2004; Orr et al. 2005). In January the waters of the study area were cold ($< 0^{\circ}C$) with relatively low pCO_2 ($< 300 \times 10^{-1}$ Pa) and characterized by a Revelle factor near 15. In March (near DOY 75) there was a significant increase in surface salinity (*see* Fig. 6b) attributed to brine rejection. It resulted in an increase in pCO_2 on the order of 30×10^{-1} Pa and a parallel increase in the Revelle factor. The effect of brine rejection is also seen in the (uncorrected) air–sea CO_2 flux estimate for the month of March, which is less than half of the value of the February flux due to the decrease in ΔpCO_2 brought about by the injection of DIC-rich, brine to the surface waters (Fig. 9). Over the same period, there was a further increase in pCO_2 of roughly 20×10^{-1} Pa attributed to respiration, which increased DIC by roughly 7 μmol kg^{-1} between February and March. In April (after DOY 100) the growth of under-ice algae reduced DIC concentrations by roughly 20 μmol kg^{-1} (or roughly 1.1 mol C m^{-2} over the month; *see* Fig. 10), reducing surface pCO_2 (and ΔpCO_2) by 30×10^{-1} Pa to 50×10^{-1} Pa, and increasing the (uncorrected) April air–sea flux (*see* Fig. 9). In June (after DOY 200), and through July and August, ice-melt is followed by the open-water phytoplankton bloom. The open-water bloom was coincident with the warming of the surface waters (Fig. 6b) and in June, the biologically mediated reduction in pCO_2 ($\sim 40 \times 10^{-1}$ Pa) was dominated by the increase in pCO_2 ($\sim 90 \times 10^{-1}$ Pa) caused by warming (*see* Fig. 6e). Over the summer period, the lowest Revelle factors (< 14) were observed (*see* Fig. 6h). This is due primarily to the decrease in the ratio of DIC : TA in the surface waters resulting from the removal of DIC (42 μmol kg^{-1}, or 2.1 mol C m^{-2} from Jun through Aug; *see* Figs. 8a, 10) by primary production. The capacity of the surface waters in Amundsen Gulf to absorb atmospheric CO_2 was, therefore, greatest during the open-water bloom, despite the fact that the water temperature was at a maximum during this period, suppressing some of this potential absorption (Fig. 9). In September (following DOY 250), and through the remainder of the year, the surface waters cooled, and the pCO_2 decreased.

Yager et al. (1995) proposed a 'seasonal rectification hypothesis' to describe the CO_2 dynamics in the Northeast water polynya with a possible extrapolation to other Arctic polynya and shelf regions (Bates 2006). This hypothesis requires that the summer season be dominated by CO_2 uptake by phytoplankton in the surface water, followed by a replenishment of CO_2 from the atmosphere by strong winds in autumn before sea-ice formation (Yager et al. 1995). The organic matter generated by the summer production is retained in the mixed-layer and remineralized in winter such that the mixed-layer becomes supersaturated with respect to atmospheric CO_2, and at which time sea-ice provides a barrier to out-gassing. The growth of ice-algae in the following early spring is then supported by this respiratory carbon (Yager et al. 1995) and followed by the open-water bloom that occurs under strong surface stratification due to the delivery of ice-melt. The inorganic carbon system in Amundsen Gulf displays some similarities to the annual process described by Yager et al. (1995): saturation with respect to atmospheric CO_2 was observed in winter only briefly as a result of brine rejection during ice formation, and organic matter respiration, both increasing DIC and pCO_2 in the surface waters. While there is evidence of respiration, or remineralization of organic carbon, in winter (Figs. 8a, 10), this accounted for only half of the organic matter produced, while the rest was vertically exported, and was not sufficient to increase pCO_2 above the atmospheric concentration. Most of the annual influx of atmospheric CO_2 ($F_{CO_2} = 1.2$ mol C m^{-2} yr^{-1}) occurred between May and October; over the same 6-month period NCP was roughly 2.4 mol C m^{-2}. The annual uptake of atmospheric CO_2 was equal to roughly 60% of the annual (net) production (NCP = 2.1 mol C m^{-2} yr^{-1}). In Amundsen Gulf, pCO_2 was depressed by primary production both by under-ice algae in spring, and by the open-water phytoplankton bloom in summer. The warming of the surface waters hindered the open-water sink for atmospheric pCO_2. During the ice-covered periods, the cold surface waters remained undersat-

urated despite the partial rectification of pCO_2 by respiration of organic matter.

A high-resolution time series covering, for the first time, a full annual cycle, in an Arctic continental shelf region has allowed us to assess processes controlling the seasonal variability of mixed-layer and subsurface carbonate system parameters, revealing an autotrophic surface layer, but a net heterotrophic system in Amundsen Gulf. The cold, relatively low-salinity surface waters were undersaturated with respect to atmospheric CO_2 throughout the year. The melting and formation of sea-ice strongly controlled the properties of the surface mixed-layer. The DIC draw-down by under-ice algae began in early April, and was followed by the spring phytoplankton bloom, which occurred after the ice break-up and the return of sunlight to the region. During the spring bloom, DIC and nitrate were consumed in roughly Redfield proportions; postbloom DIC draw-down, and corresponding production of DOC, continued in non–Redfield proportions under nutrient-limited conditions. We estimated that roughly 30% of NCP (computed from inorganic carbon) was converted to DOC in the surface mixed-layer. Respiration in the subsurface layer exceeded the estimated surface production and is, therefore, likely supported by inorganic carbon generated by benthic respiration.

Acknowledgments

We are grateful to the captains, officers, and crew of the Canadian Coast Guard Ship *Amundsen* for their cooperation in the collection of field data, and also to the chief scientists throughout the project. We thank Yves Gratton and his team of rosette operators for the collection and distribution of hydrographic data. Many thanks to Friederike Prowe, Stelly Lefort, Constance Guignard, Nes Sutherland, Stephanie Moore, and Doris Leong for their assistance with sample collection and analysis. We are grateful to two anonymous reviewers and to Nick Bates for their insightful comments. This work was supported by the Swedish Research Council, the Royal Society of Arts and Sciences in Göteborg, the Canadian Natural Science and Engineering Research Council, ArcticNet, and MetOcean Data Systems. This research contributes to the Canadian International Polar Year initiatives, as part of the Circumpolar Flaw Lead System Study project, and to the International Geosphere Biosphere Programme/International Human Dimensions Programme, and to Land Ocean Interactions in the Coastal Zone.

References

Aagaard, K. 1984. The Beaufort undercurrent, p. 47–71. *In* P. Barnes and E. Reimnitz [eds.], The Alaskan Beaufort Sea: Ecosystems and environments. Academic Press.

———, and E. C. Carmack. 1994. The Arctic Ocean and climate: A perspective, p. 5–20. In O. M. Johannessen, R. D. Muench, and J. E. Overland [eds.], The Polar Oceans and their role in shaping the global environment. American Geophysical Union.

———, L. K. Coachman, and E. C. Carmack. 1981. On the halocline of the Arctic Ocean. Deep-Sea Res. **28:** 529–545.

Alonso-Sáez, L., O. Sánchez, J. M. Gasol, V. Balagué, and C. Pédros-Alio. 2008. Winter-to-summer changes in the composition and single-cell activity of near-surface Arctic prokaryotes. Environ. Microbiol. **10:** 2444–2454, doi:10.1111/j.1462-2920.2008.01674.x

Arrigo, K. R. 2005. Marine microorganisms and global nutrient cycles. Nature **437:** 349–355, doi:10.1038/nature04159

———, and G. L. van Dijken. 2004. Annual cycles of sea ice and phytoplankton in Cape Bathurst polynya, southeastern Beaufort Sea, Canadian Arctic. Geophys. Res. Lett. **31:** L08304, doi:10.1029/2003GL018978

Barber, D. G., and R. Massom. 2006. The role off sea ice in bipolar polynya processes. Elsevier Oceanography Series.

Bates, N. R. 2006. Air–sea CO_2 fluxes and the continental shelf pump of carbon in the Chukchi Sea adjacent to the Arctic Ocean. J. Geophys. Res. **111:** C10013, doi:10.1029/2005JC003083

———. 2007. Interannual variability of the oceanic CO_2 sink in the subtropical gyre of the North Atlantic over the last 2 decades. J. Geophys. Res. **112:** C09013, doi:10.1029/2006JC003759

———, and J. T. Mathis. 2009. The Arctic Ocean marine carbon cycle: Evaluation of air–sea CO_2 exchanges, ocean acidification impacts and potential feedbacks. Biogeosciences **6:** 2433–2459, doi:10.5194/bg-6-2433-2009

———, ———, and L. Cooper. 2009. The effect ocean acidification on biologically induced seasonality of carbonate mineral saturation states in the western Arctic. J. Geophys. Res. **114:** C11007, doi:10.1029/2008JC004862

———, A. F. Michaels, and A. H. Knap. 1996. Seasonal and interannual variability of oceanic carbon dioxide species at the U.S. JGOFS Bermuda Atlantic time-series study (BATS) site. Deep-Sea Res. Part II **43:** 347–383, doi:10.1016/0967-0645(95)00093-3

Borges, A. V. 2005. Do we have enough pieces of the jigsaw to integrate CO_2 fluxes in the coastal ocean? Estuaries **28:** 3–27, doi:10.1007/BF02732750

———, B. Delille, and M. Frankignoulle. 2005. Budgeting sinks and sources of CO_2 in the coastal ocean: Diversity of ecosystems counts. Geophys. Res. Lett. **32:** L14601, doi:10.1029/2005GL023053

Bozec, Y., H. Thomas, K. Elkalay, and H. J. W. de Baar. 2005. The continental shelf pump for CO_2 in the North Sea—evidence from summer observation. Mar. Chem. **93:** 131–147, doi:10.1016/j.marchem.2004.07.006

———, ———, L.-S. Schiettecatte, A. V. Borges, K. Elkalay, and H. J. W. de Baar. 2006. Assessment of the processes controlling seasonal variations of dissolved inorganic carbon in the North Sea. Limnol. Oceanogr. **51:** 2746–2762, doi:10.4319/lo.2006.51.6.2746

Carmack, E. C., and R. W. Macdonald. 2002. Oceanography of the Canadian Shelf of the Beaufort Sea: A setting for marine life. Arctic **55:** 29–45.

Chen, C.-T. A., and A. V. Borges. 2009. Reconciling opposing views on carbon cycling in the coastal ocean: Continental shelves as sinks and near-shore ecosystems as sources of atmospheric CO_2. Deep-Sea Res. Part II **33:** L12603, doi:10.1016/j.dsr2.2009.01.001.

Chierici, M., and A. Fransson. 2009. Calcium carbonate saturation in the surface water of the Arctic Ocean: Undersaturation in freshwater influenced shelves. Biogeosciences **6:** 2421–2432, doi:10.5194/bg-6-2421-2009

Dickson, A. G., and F. J. Millero. 1987. A comparison of the equilibrium constants for the dissociation of carbonic acid in seawater media. Deep-Sea Res. Part I **34:** 1733–1743, doi:10.1016/0198-0149(87)90021-5

———, C. L. Sabine, and J. R. Christian. 2007. Guide to best practices for ocean CO_2 measurements. PICES Special Publication **3**.

Fennel, K., J. Wilkin, M. Previdi, and R. Najjar. 2008. Denitrification effects on air–sea CO_2 flux in the coastal ocean: Simulations for the northwest North Atlantic. Geophys. Res. Lett. **35:** L24608, doi:10.1029/2008GL036147

Forest, A., and others. 2008. The annual cycle of particulate organic carbon export in Franklin Bay (Canadian Arctic): Environmental control and food web implications. J. Geophys. Res. **113:** C03S05, doi:10.1029/2007JC004262

Frankignoulle, M., and A. V. Borges. 2001. European continental shelf as a significant sink for atmospheric carbon dioxide. Glob. Biogeochem. Cycles **15:** 569–576, doi:10.1029/2000GB001307

Garneau, M.-E., S. Roy, C. Lovejoy, Y. Gratton, and W. F. Vincent. 2008. Seasonal dynamics of bacterial biomass and production in a coastal Arctic ecosystem: Franklin Bay, western Canadian Arctic. J. Geophys. Res. **113:** C07S91, doi:10.1029/2007JC004281

Gosselin, M., M. Levasseur, P. A. Wheeler, R. A. Horner, and B. C. Booth. 1997. New measurements of phytoplankton and ice algal production in the Arctic Ocean. Deep-Sea Res. Part II **44:** 1623–1644, doi:10.1016/S0967-0645(97)00054-4

Gradinger, R. 1996. Occurrence of an algal bloom under Arctic pack ice. Mar. Ecol. Prog. Ser. **131:** 301–305, doi:10.3354/meps131301

Grasshoff, K. 1999. Methods of seawater analyses. Weinheim.

Hansell, D. A., and C. A. Carlson. 2001. Marine dissolved organic matter and the carbon cycle. Oceanography **14:** 41–49.

———, D. Kadko, and N. R. Bates. 2004. Degradation of terrigenous dissolved organic carbon in the western Arctic Ocean. Science **304:** 858–861, doi:10.1126/science.1096175

Horner, R., and G. C. Schrader. 1982. Relative contributions of ice algae, phytoplankton, and benthic microalgae to primary production in nearshore regions of the Beaufort Sea. Arctic **35:** 485–503.

Hutchins, D. A., and K. W. Bruland. 1998. Iron-limited diatom growth and Si : N uptake ratios in a coastal upwelling regime. Nature **393:** 561–564, doi:10.1038/31203

Johnson, K. M., K. D. Wills, D. B. Butler, W. K. Johnson, and C. S. Wong. 1993. Coulometric total carbon dioxide analysis for marine studies: Maximizing the performance of an automated gas extraction system and coulometric detector. Mar. Chem. **44:** 167–188, doi:10.1016/0304-4203(93)90201-X

Jull-Pedersen, T., C. Michel, and M. Gosselin. 2010. Sinking export of particulate organic material from the euphotic zone in the eastern Beaufort Sea. Mar. Ecol. Prog. Ser. **410:** 55–70, doi:10.3354/meps08608

Körtzinger, A., H. Thomas, B. Schneider, N. Gronau, L. Mintrop, and J. C. Duinker. 1996. At-sea intercomparison of two newly designed underway pCO_2 systems—encouraging results. Mar. Chem. **52:** 133–145, doi:10.1016/0304-4203(95)00083-6

Lanos, R. 2009. Circulation régionale, masses d'eau, cycles d'évolution et transports entre la mer de Beaufort et le Golfe d'Amundsen. Ph.D. thesis. Univérsité du Québec. [Regional circulation, water masses, cycles of evolution and transport between the Beaufort Sea and Amundsen Gulf.]

Lewis, E., and D. W. R. Wallace. 1998. Program developed for CO_2 systems calculations. ORNL/CDIAC **105**, Carbon Dioxide Information Analysis Center, Oak Ridge National Laboratory, U.S. Department of Energy.

Loose, B., W. R. McGillis, P. Schlosser, D. Perovich, and T. Takahashi. 2009. Effects of freezing, growth, and ice cover on gas transport processes in laboratory seawater experiments. Geophys. Res. Lett. **36:** L05603, doi:10.1029/2008GL036318

Macdonald, R. W., F. A. McLaughlin, and E. C. Carmack. 2002. Fresh water and its sources during the SHEBA drift in the Canada Basin of the Arctic Ocean. Deep-Sea Res. Part I. **49:** 1769–1785, doi:10.1016/S0967-0637(02)00097-3

———, S. M. Soloman, R. E. Cranston, H. E. Welch, and M. B. Yunker. 1998. A sediment and organic carbon budget for the Canadian Beaufort Shelf. Mar. Geol. **144:** 255–273, doi:10.1016/S0025-3227(97)00106-0

———, C. S. Wong, and P. E. Erickson. 1987. The distribution of nutrients in the southeastern Beaufort Sea: Implications for water circulation and primary production. J. Geophys. Res. **92:** 2939–2952, doi:10.1029/JC092iC03p02939

Magen, C., and others. 2010. Origin and fate of particulate organic matter in the southern Beaufort Sea–Amundsen Gulf region, Canadian Arctic. Estuar. Coast. Shelf Sci. **86:** 31–41, doi:10.1016/j.ecss.2009.09.009

Maslanik, J. A., C. Fowler, J. Stroeve, S. Drobot, J. Zwally, D. Yi, and W. Emery. 2007. A younger, thinner Arctic ice cover: Increased potential for rapid, extensive sea-ice loss. Geophys. Res. Lett. **34:** L24501, doi:10.1029/2007GL032043

Mathis, J. T., D. A. Hansell, and N. R. Bates. 2005. Strong hydrographic controls on spatial and seasonal variability of dissolved organic carbon in the Chukchi Sea. Deep-Sea Res. Part II **52:** 3245–3258, doi:10.1016/j.dsr2.2005.10.002

———, ———, D. Kadko, N. R. Bates, and L. W. Cooper. 2007. Determining net dissolved organic carbon production in the hydrographically complex western Arctic Ocean. Limnol. Oceanogr. **52:** 1789–1799.

McLaughlin, F. A., E. C. Carmack, R. G. Ingram, W. J. Williams, and C. Michel. 2005. Oceanography of the Northwest Passage, p. 1213–1244. *In* A. R. Robinson and K. Brink [eds.], The Sea. V. 14. The global coastal ocean. Harvard Univ. Press.

———, and others. 2004. The joint roles of Pacific and Atlantic-origin waters in the Canada Basin, 1997–1998. Deep-Sea Res. Part I **51:** 107–128, doi:10.1016/j.dsr.2003.09.010

Mehrbach, C., C. H. Culberson, J. E. Hawley, and R. M. Pytkowicz. 1973. Measurement of the apparent dissociation constants of carbonic acid in seawater at atmospheric pressure. Limnol. Oceanogr. **18:** 897–907, doi:10.4319/lo.1973.18.6.0897

Meincke, J., B. Rudels, and H. J. Friedrich. 1997. The Arctic Ocean–Nordic Seas thermohaline system. J. Mar. Sci. **54:** 283–299.

Melling, H. 1993. The formation of a haline shelf front in wintertime in an ice-covered Arctic sea. Continent. Shelf Res. **13:** 1123–1147, doi:10.1016/0278-4343(93)90045-Y

Moritz, R. E., C. M. Bitz, and E. J. Steig. 2002. Dynamics of recent climate change in the Arctic. Science **297:** 1497–1502, doi:10.1126/science.1076522

Mucci, A., and others. 2008. Organic and inorganic fluxes, p. 113–142. *In* L. Fortier, D. Barber, and J. Michaud [eds.], On thin ice: A synthesis of the Canadian Arctic Shelf Exchange Study (CASES). Aboriginal Issue Press.

———, B. Lansard, L. A. Miller, and T. N. Papakyriakou. 2010. CO_2 fluxes across the air–sea interface in the southeastern Beaufort Sea: The ice-free period. J. Geophys. Res. **297:** 1497–1502.

Munk, W. H. 1966. Abyssal recipes. Deep-Sea Res. **13:** 709–730.

Naegler, T., P. Ciais, K. Rodgers, and I. Levin. 2006. Excess radiocarbon constraints on air–sea gas exchange and the uptake of CO_2 by the oceans. Geophys. Res. Lett. **33:** L11802, doi:10.1029/2005GL025408

Olsen, A., K. R. Brown, M. Chierici, T. Johannessen, and C. Neill. 2008. Sea-surface CO_2 fugacity in the subpolar North Atlantic. Biogeosciences **5:** 535–547, doi:10.5194/bg-5-535-2008

Omar, A. M., A. Olsen, T. Johannessen, M. Hoppema, H. Thomas, and A. V. Borges. 2010. Spatiotemporal variations of fCO_2 in the North Sea. Ocean Sci. **6:** 77–89, doi:10.5194/os-6-77-2010

Orr, J. C., and others. 2005. Anthropogenic ocean acidification over the twenty-first century and its impact on calcifying organisms. Nature **437:** 681–686, doi:10.1038/nature04095

Renaud, P. E., A. Riedel, C. Michel, N. Morata, M. Gosselin, T. Juul-Pedersen, and A. Chiuchiolo. 2007. Seasonal variation in benthic community oxygen demand: A response to an ice algal bloom in the Beaufort Sea, Canadian Arctic? J. Mar. Sys. **67:** 1–12, doi:10.1016/j.jmarsys.2006.07.006

Revelle, R., and H. E. Suess. 1957. Carbon dioxide exchange between atmosphere and ocean and the question of an increase of atmospheric CO_2 during the past decades. Tellus **9:** 18–27, doi:10.1111/j.2153-3490.1957.tb01849.x

Richerol, T., A. Rochon, S. Blasco, D. B. Scott, T. M. Schell, and R. J. Bennett. 2008. Distribution of dinoflagellate cysts in surface sediments of the Mackenzie Shelf and Amundsen Gulf, Beaufort Sea (Canada). J. Mar. Sys. **74:** 825–839, doi:10.1016/j.jmarsys.2007.11.003

Riedel, A., C. Michel, and M. Gosselin. 2006. Seasonal study of sea-ice exopolymeric substances on the Mackenzie Shelf: Implications for transport of sea-ice bacteria and algae. Mar. Ecol. Prog. Ser. **45:** 195–206.

———, ———, ———, and B. Leblanc. 2008. Winter–spring dynamics in sea-ice carbon cycling in the coastal Arctic Ocean. J. Mar. Sys. **74:** 918–932, doi:10.1016/j.jmarsys.2008.01.003

Rudels, B., L. G. Anderson, and E. P. Jones. 1996. Formation and evolution of the surface mixed layer and halocline of the Arctic Ocean. J. Geophys. Res. **101:** 8807–8821, doi:10.1029/96JC00143

Sabine, C. L., and others. 2004. The oceanic sink for anthropogenic CO_2. Science **305:** 367–371, doi:10.1126/science.1097403

Semiletov, I., A. Makshtas, S.-I. Akasofu, and E. Andreas. 2004. Atmospheric CO_2 balance: The role of Arctic sea ice. Geophys. Res. Lett. **31:** L05121, doi:10.1029/2003GL017996

Serreze, M. C., and others. 2000. Observational evidence of recent change in the northern high-latitude environment. Clim. Change **46:** 159–207, doi:10.1023/A:1005504031923

Stewart, R. E., and others. 1998. The Mackenzie GEWEX study: The water and energy cycles of a major North American river basin. Bull. Am. Meteorol. Soc. **79:** 2665–2683, doi:10.1175/1520-0477(1998)079<2665:TMGSTW>2.0.CO;2

Stroeve, J., M. M. Holland, W. Meier, T. Scambos, and M. Serreze. 2007. Arctic sea ice decline: Faster than forecast. Geophys. Res. Lett. **34:** L09501, doi:10.1029/2007GL029703

Sweeney, C., E. Gloor, A. R. Jacobson, R. M. Key, G. McKinley, J. L. Sarmiento, and R. Wanninkhof. 2007. Constraining global air–sea gas exchange for CO_2 with recent bomb ^{14}C measurements. Glob. Biogeochem. Cycles **21:** GB2015, doi:10.1029/2006GB002784

Takahashi, T., J. Olafsson, J. G. Goddard, D. W. Chipman, and S. G. Sutherland. 1993. Seasonal variation of CO_2 and nutrients in the high-latitude surface oceans: A comparative study. Glob. Biocheochem. Cycles **7:** 843–878, doi:10.1029/93GB02263

———, and others. 2002. Global sea–air CO_2 flux based on climatological surface ocean pCO_2, and seasonal biological and temperature effects. Deep-Sea Res. Part II **49:** 1601–1622, doi:10.1016/S0967-0645(02)00003-6

Takeda, S. 1998. Influence of iron availability on nutrient consumption ratio of diatoms in oceanic waters. Nature **393:** 774–777, doi:10.1038/31674

Thomas, H., and others. 2005. The carbon budget of the North Sea. Biogeosciences **2:** 87–96, doi:10.5194/bg-2-87-2005

———, V. Ittekkot, C. Osterroht, and B. Schneider. 1999. Preferential recycling of nutrients—the ocean's way to increase new production and to pass nutrient limitation? Limnol. Oceanogr. **44:** 1999–2004, doi:10.4319/lo.1999.44.8.1999

———, and others. 2007. Rapid decline of the CO_2 buffering capacity in the North Sea and implications for the North Atlantic Ocean. Glob. Biogeochem. Cycles **21:** GB4001, doi:10.1029/2006GB002825

———, and ———. 2009. Enhanced ocean carbon storage from anaerobic alkalinity generation in coastal sediments. Biogeosciences **6:** 267–274, doi:10.5194/bg-6-267-2009

———, and B. Schneider. 1999. The seasonal cycle of carbon dioxide in Baltic Sea surface waters. J. Mar. Syst. **22:** 53–67, doi:10.1016/S0924-7963(99)00030-5

Tremblay, J.-É., K. Simpson, J. Martin, L. M. Y. Gratton, D. Barber, and N. M. Price. 2008. Vertical stability and the annual dynamics of nutrients and chlorophyll fluorescence in the coastal, southeast Beaufort Sea. J. Geophys. Res. **113:** C07S90, doi:10.1029/2007JC004547

Vallières, C., L. Retamal, P. Ramlal, C. L. Osburn, and W. F. Vincent. 2008. Bacterial production and microbial food web structure in a large Arctic river and the coastal Arctic Ocean. J. Mar. Syst. **74:** 756–773, doi:10.1016/j.jmarsys.2007.12.002

Walsh, J. J. 1991. Importance of continental margins in the marine biogeochemical cycling of carbon and nitrogen. Nature **350:** 753–55, doi:10.1038/350053a0

Wanninkhof, R. 1992. Relationships between wind speed and gas exchange over the ocean. J. Geophys. Res. **97:** 7373–7382, doi:10.1029/92JC00188

Watson, A. J., and others. 2009. Tracking the variable North Atlantic sink for atmospheric CO_2. Science **326:** 1391–1393, doi:10.1126/science.1177394

Weiss, R. F., R. A. Jahnke, and C. D. Keeling. 1982. Seasonal effects of temperature and salinity on the partial pressure of CO_2 in seawater. Nature **300:** 511–513, doi:10.1038/300511a0

Yager, P. L., D. W. R. Wallace, K. M. Johnson, W. O. Smith, Jr., P. J. Minnett, and J. W. Deming. 1995. The Northeast Water Polynya as an atmospheric CO_2 sink: A seasonal rectification hypothesis. J. Geophys. Res. **100:** 4389–4398, doi:10.1029/94JC01962

Yamamoto-Kawai, M., and N. Tanaka. 2005. Freshwater and brine behaviors in the Arctic Ocean deduced from historical data of $\Delta^{18}O$ and alkalinity (1992–2002 a.d.). J. Geophys. Res. **1110:** C10003, doi:10.1029/2004JC002793

Associate editor: Mary I. Scranton

Received: 01 May 2010
Accepted: 14 October 2010
Amended: 28 October 2010